Inorganic Chemistry

Article

pubs.acs.org/IC

Photophysical Responses in Pt_2Pb Clusters Driven by Solvent Interactions and Structural Changes in the Pb^{II} Environment

Jesús R. Berenguer,[†] Elena Lalinde,*[,†] Antonio Martín,[‡] M. Teresa Moreno,*[,†] Santiago Ruiz,[†] Sergio Sánchez,[§] and Hamid R. Shahsavari[†,∥]

[†]Departamento de Química-Centro de Síntesis Química de La Rioja (CISQ), Universidad de La Rioja, Madre de Dios, 51, 26006 Logroño, Spain

[‡]Departamento de Química Inorgánica, Instituto de Ciencia de Materiales de Aragón, Facultad de Ciencias, Universidad de Zaragoza-CSIC, Plaza S. Francisco s/n 50009 Zaragoza, Spain

[§]School of Chemistry, University of Manchester, Oxford Road, Manchester M13 9PL, U.K.

Supporting Information

ABSTRACT: Two types of Pt_2Pb luminescent clusters were successfully prepared by the reaction of $[Pt(C_6F_5)(bzq)(OCMe_2)]$ (**1**) and $[Pt(C_6F_5)(ppy)(dmso)]$ (**2**) with $[Pb(SpyR\text{-}5)_2]$ (R = H, CF_3). Thus, whereas **5** (ppy, Spy) is generated through coordination of the pyridine-N atoms to the Pt centers, the formation of **3**, **4** (bzq), and **6** (ppy, $SpyCF_3$) is accompanied by a formal thiolate transfer from Pb^{II} to Pt^{II}, keeping the two N atoms in the primary environment of the lead. In **5**, the *neutral* Pb center adopts a rather stable and symmetrical "Pt_2S_2" coordination sphere supplemented by two Pb··F_o contacts, whereas for the remaining species several pseudopolymorphs were found depending on the solvent (**3**, **4**) and crystallization conditions (**6**). This structural diversity relies on changes in the coordination mode of the SpyR ligands (μ-$\kappa S,N/\mu$-$\kappa^3 S,N,S$), intermetallic Pt−Pb bonds, and secondary *intra-* and *intermolecular* contacts induced by Pb−solvent binding. Notably, the changes, which entail a slight tuning of the stereochemical activity of the lone pair, have also a remarkable impact on the emissive state (^{3}L′CCT/^{3}L′LCT, SpyR → Pb,Pt/(C^N) in nature). Clusters **3** and **4** display a distinct and fast reversible blue shift vapoluminescent response (**4** shows also color changes) to donor solvents, correlated with changes in the environment of the Pb^{II} ion (asymmetric *hemidirected* to more symmetric *holodirected*) upon solvent binding and, additionally, in **4** with modifications in the crystal packing, as confirmed by XRD and supported by TD-DFT calculations. **5** and **6** do not show a vapoluminescent response. However, for **6**, three different and interconvertible forms, a symmetrical form (yellow **6-y**) and two asymmetrical forms with a rather short Pt−Pb bond (pale orange **6·acetone** and orange **6-o**), exhibiting different emissions were found. Notably, slow crystallization and low concentration favor the formation of the *thermodynamically* more stable yellow form, whereas fast crystallization gives rise to orange solids with a remarkable red shift of the emission. Interestingly, **6** also exhibits reversible *mechanochromic* color and luminescence changes.

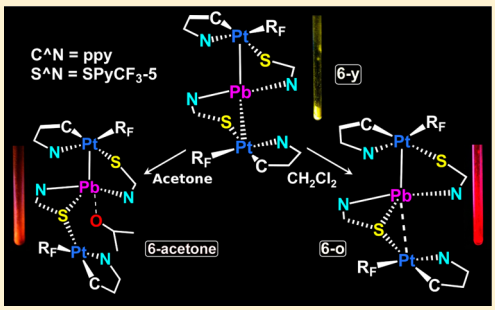

INTRODUCTION

The design and preparation of polynuclear and cluster complexes containing dative or covalent metal−metal bonds is an active research field due not only to their interesting structures and bonding features[1] but also to their intrinsic properties with potential application in molecular electronics and materials science.[2] Metallophilic interactions involving closed-shell metal ions have been prominent in this regard, and their role in stabilizing supramolecular networks[3] and in their unusual associated optical properties, in both solution[4] and the solid state is now well recognized.[2a,b,d,4d,5] In this regard, considerable efforts have been made in the preparation of molecular architectures containing d^{10} [5a−h] and d^8 ions[4d,5d,i,j] (or a combination of both in heterometallic systems)[2b,d,5k−p,6] and the study of their luminescent properties. Notably, in the solid state, the photophysical behavior of some of these systems has been found to be sensitive to external stimuli such as VOCs (vapoluminescence),[5d,7] mechanical grinding (mechanochromism),[8] or temperature (thermochromism),[9] which is particularly relevant to the development of novel photofunctional materials. These phenomena have been usually correlated with subtle structural transformations, which are often associated with the formation/disruption or modification of metal−metal interactions or interligand $\pi\cdots\pi$ stacking, although for polymetallic systems exhibiting response to vapors, metal−ligand coordination/decoordination has been also demonstrated.[10]

Within this framework, heteropolynuclear systems incorporating heavy metals with a $d^{10}s^2$ valence shell (Tl^I, Pb^{II}) have been comparatively much less explored. In the case of thallium, following the pioneering contribution of the first luminescent Pt^{II}−T^{II} complex $Tl_2Pt(CN)_4$,[11] interesting families of hetero-

Received: June 19, 2014
Published: August 5, 2014

   dx.doi.org/10.1021/ic501458q | Inorg. Chem. 2014, 53, 8770−8785

nuclear M−Tl^I complexes, mainly with platinum(0,II)[9b,c,12] and gold(I),[5l,m,13] having diverse structural configurations and exhibiting intriguing photophysical properties have been also reported. In contrast, the number of polymetallic systems involving the harder Pb^{2+} ion in metallophilic interactions is quite limited,[12r,14] and still little is known about their photoluminescence properties.[14d,e] In these heterometallic systems, the $6s^2$ electron lone pair of the heavy ion (Tl^I, Pb^{II}) usually exerts a remarkable structural influence, depending on its stereoactivity.[15] This electronic and structural effect, attributed to ligand-to-metal charge transfer, is particularly relevant in lead(II)-containing systems due to its higher charge, thus favoring the formation of more or less *hemidirectional* environments having a void in the coordination sphere of the Pb^{II}, which is occupied by the stereochemically active lone pair.

We are interested in preparing platinum−lead(II) systems due to the well-known capacity of Pb^{II} to adopt a wide range of coordination numbers (from 2 to 12) and geometries arising from subtle changes in the stereochemical activity of the lone pair.[15] In particular, when the lone pair is active, it is expected that its degree of activity will be susceptible to the influence of external factors (binding of vapors, mechanical forces, ...) with concomitant changes in electronic structure and properties. This structural property might endow these Pt^{II}−Pb^{II} complexes with some unique properties, such as the response to external stimuli, thereby providing the opportunity of forming dynamic stimuli-responsive materials. By using alkynyl platinates as basic building bloks and the $Pb(ClO_4)_2{\cdot}3H_2O$ salt, we have successfully prepared several sandwich-type trinuclear Pt_2Pb[16] and tetranuclear Pt_2Pb_2[17] clusters, stabilized by a synergistic combination of η^1 and/or η^2 $Pb^{II}\cdots(C{\equiv}CR)$ and Pt^{II}−Pb^{II} bonding interactions, which have been demonstrated to display interesting photophysical properties depending on the topology and the alkynyl substituents. Notably, the emissive tetranuclear clusters $[Pt_2Pb_2(C{\equiv}CR)_8]$ (R = Tol, C_6H_4OMe-3)[17] have a rather dynamic core sensitive to mechanical grinding and donor solvents. In particular, the remarkable and distinct vapochromic response observed has been ascribed to a fast creation/disruption of Pb−solvate clusters $[Pt_2Pb_2(C{\equiv}CR)_8S_x]$ (S = donor volatile, $x \geq 2$) with concomitant geometrical and electronic changes.

In the search for new and more robust platinum−lead systems, we considered it of interest to explore its formation by self-assembly of neutral building precursors. In a recent communication, we reported the preparation of the very stable Pt_2Pb cluster $[\{Pt(C_6F_5)(bzq)\}_2Pb(Spy)_2]$ (**3**; bzq = benzoquinolinyl, Spy^- = 2-pyridinethiolate) by reaction of the acetone solvate $[Pt(C_6F_5)(bzq)(OCMe_2)]$ with $[Pb(Spy)_2]$.[18] This cluster features two distinct Pt−Pb bonds supported by two different bridging pyridine-2-thiolate ligands (μ-$\kappa S,N$ and μ-$\kappa^3 S,N,S$) and modulates its vapoluminescent response toward different organic oxygen donor solvents (O) through solvent-induced reversible intercluster changes, involving a change from a local Pt_2N_2S environment around the Pb^{II} ion in the free solvent **3** to Pt_2N_2O in the solvate **3·acetone** (Chart 1).[18] Intrigued by this unique behavior, we decided to study the role of the cycloplatinated "Pt(C^N)" fragment and the basicity of the ancillary thiolate bridging ligand in the structures and photophysical behavior of these heterometallic systems. Herein, we report the synthesis, spectroscopic and structural characterization, and photophysical studies of a series of new luminescent Pt_2Pb clusters, $[\{Pt(C_6F_5)(C^N)\}_2Pb(SpyR\text{-}5)_2]$ (**3**−**6**; C^N = bzq, ppy, R = H, CF_3). The related bzq/$SpyCF_3$ complex **4** exhibited vapochromic behavior with response in color and luminescence, while the ppy/SpyR-5 derivative **5** (R = H), which displays a symmetrical PbS_2Pt_2 core, and **6** (R = CF_3) did not show vapochromic behavior. In the case of **6** its structure and properties were found to depend on the crystallization conditions, and it also displayed mechanochromic properties. To get insight into the nature of their photophysical properties, TD-DFT calculations were carried out in the gas phase on some selected unsolvated and solvated clusters.

Chart 1

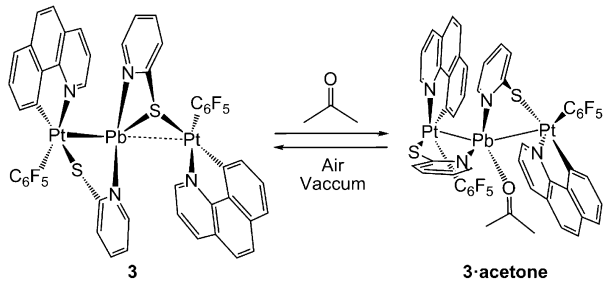

RESULTS AND DISCUSSION

Synthesis. The trinuclear complexes $[\{Pt(C_6F_5)(bzq)\}_2Pb(\mu\text{-}SpyR\text{-}5)_2]$ (bzq = benzoquinolinyl, R = H (**3**), CF_3 (**4**)) were obtained as orange solids by treatment of the acetone solvate $[Pt(C_6F_5)(bzq)(OCMe_2)]$ (**1**) with 0.5 equiv of the appropriate bis(pyridinethiolate)lead(II). It is worth noting that the reactions evolve with formal thiolate transfer, plausibly favored by the soft nature of Pt^{II} (Scheme 1a). The attempts to synthesize the acetone solvate $[Pt(C_6F_5)(ppy)(OCMe_2)]$ with the 2-phenylpyridine ligand (Hppy) under conditions similar to those described for **1** were unsuccessful. Fortunately, the synthesis of the targeted clusters $[\{Pt(C_6F_5)(ppy)\}_2Pb(\mu\text{-}SpyR\text{-}5)_2]$ (R = H (**5**), CF_3 (**6**)), as orange (**5**) or yellow (**6**) solids, was achieved by using the dimethyl sulfoxide solvate $[Pt(C_6F_5)(ppy)(dmso)]$ (**2**) as the precursor (Scheme 1b). Surprisingly, whereas the formation of **6** takes also place with thiolate transfer from Pb^{II} to Pt^{II}, in the case of cluster **5**, however, this transfer does not occur, keeping the sulfur coordinated to the Pb atom, as evidenced by X-ray. As shown in Scheme 1b, the precursor **2** was prepared following similar approaches to related aryl-cycloplatinate complexes, by refluxing a mixture of *cis*-$[Pt(C_6F_5)_2(dmso)_2]$ and Hppy (1 equiv) in toluene (32 h), and its structure was identified by spectroscopic means (Experimental Section) and X-ray crystallography (see below).

NMR Characterization. In solution, the most remarkable spectroscopic features of the precursor complex **2** are the high value of the ^{195}Pt−F_o coupling constant (494 Hz), consistent with the low *trans* influence of the N atom *trans* to the C_{ipso} atom of the C_6F_5 group, and the notable upfield shift of the *o*-H^9 proton of the ppy ligand (δ 6.41, $^3J_{Pt-H}$ = 62.4 Hz) due to the anisotropic effect of the C_6F_5 ring.

Complexes **3**−**6** were characterized by standard analytical and spectroscopic techniques, and their integrity in solution was confirmed by multinuclear (^1H, ^{19}F (CD_2Cl_2, CD_3COCD_3), and $^{13}C\{^1H\}$) NMR spectroscopy (assignments made on the basis of 2D experiments; schematic labeling given in Figure S1 (Supporting Information)). For all complexes **3**−**6** only one set of cyclometalated, C_6F_5, and bridging SpyR groups

dx.doi.org/10.1021/ic501458q | Inorg. Chem. 2014, 53, 8770−8785

Scheme 1

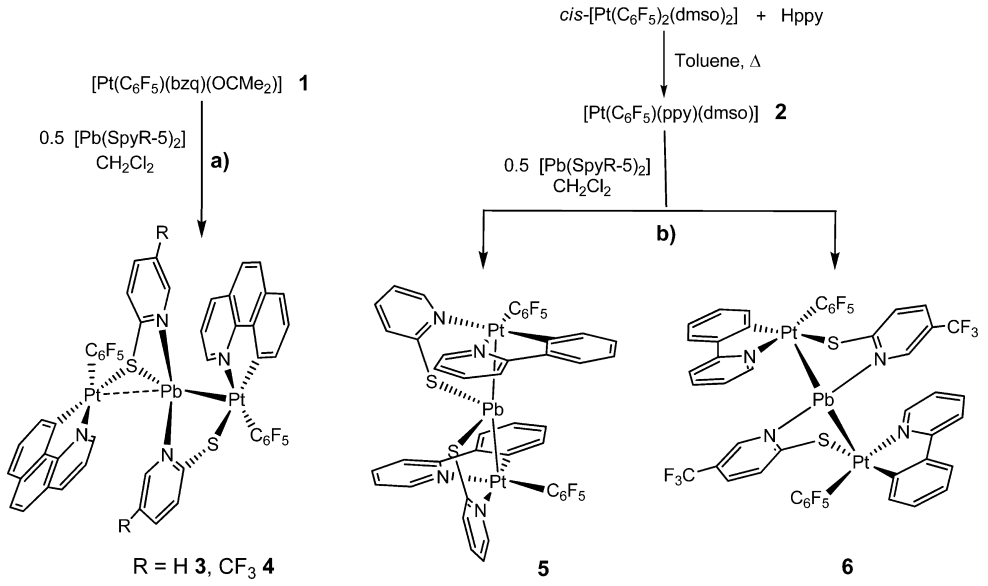

was observed, even at low temperature, indicating that the structural differences between the two "Pt(C_6F_5)(C^N)(μ-SpyR)" fragments observed in the solid state for **3**, **4**, and **6** around Pb^{II} are averaged in solution. The most relevant features are provided by ^{19}F NMR spectroscopy. In a donor solvent such as CD_3COCD_3, the complexes exhibit the typical AA′MXX′ pattern ($2F_o$, F_p, $2F_m$), revealing that the pentafluorophenyl groups have free rotation about the Pt–$C_{ipso}(C_6F_5)$ bonds. The *o*-fluorine signal is only flanked by platinum satellites, pointing to the absence of F···Pb contacts in this donor solvent. However, it is worth noting that the ^{195}Pt–F_o coupling constants (382–408 Hz) are clearly smaller than those in the starting precursors (501 Hz, **1**; 494 Hz, **2**), thus supporting the integrity of Pt^{II}–Pb^{II}–Pt^{II} bonds. The remarkable reduction in the $J^{195}_{Pt-F_o}$ value is consistent with the increase in the coordination index of the Pt center (from 4 to 5) upon formation of the Pt–Pb bonds. The ^{19}F NMR spectra were also recorded in CD_2Cl_2, revealing not only a more rigid behavior but also the persistence of close contacts Pb···F_o in solution. In this solvent, at ambient temperature, the *o*-fluorine resonances are very broad, indicative of dynamic behavior. While in complexes with the substituted $SpyCF_3$ bridging ligand (**4** and **6**) two distinct very broad signals (*exo*- and *endo*-F_o) are seen, in complexes **3** and **5** both resonances are close to $T_{coalescence}$ (**3**) or slightly up (**5** broad hump). When the temperature is lowered to 186 K, two distinct F_o (*endo* and *exo*, and also two F_m) resonances appear in all complexes **3**–**6** (see Figure S2 (Supporting Information) for **4**). The *exo*-F_o atoms appear at low field (δ −115.7 for **6** to δ −116.3 for **3**) with well-resolved platinum satellites, whereas the *endo*-F_o atoms are seen in the range δ −123.1 for **6** to −124.6 for **4**, clearly flanked in **3**–**5** by two sets of satellites due to coupling to ^{207}Pb and ^{195}Pt, respectively (see Figure 1 for **4**). The *endo*-fluorine–lead coupling constants ($J^{207}_{Pb-^{19}F}$ = 1564 (**3**), 1594 (**4**), and 1557 Hz (**5**)) are larger than that previously reported for the tetranuclear anion $[Pb\{Pt(\mu\text{-}Cl)(C_6F_5)_2\}_3]^-$ (1140 Hz),[14d] which also displays close F_o···Pb contacts. Interestingly, the presence of these *endo*-F_o···Pb contacts is also reflected in the corresponding values of coupling constants $^3J_{Pt-F_{o(endo)}}$ (289–317 Hz), which decrease in relation to those observed for the *exo*-F_o (384–404 Hz).

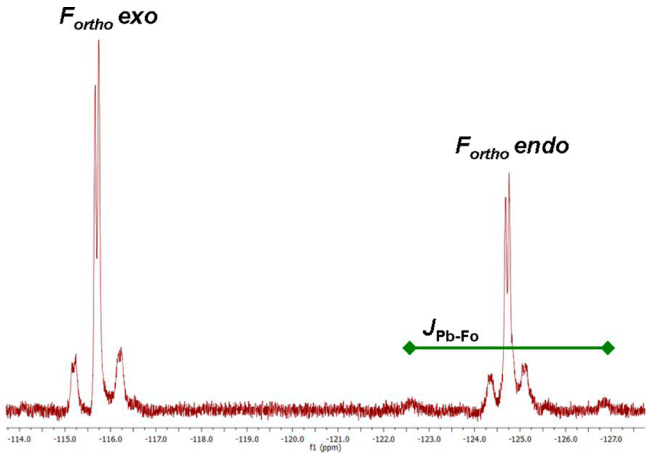

Figure 1. *o*-F region in the ^{19}F NMR spectrum of **4** in CD_2Cl_2 at 186 K.

X-ray Diffraction. Complex **2** (Figure 2, Table S1 (Supporting Information)) exhibits the expected square-planar environment around platinum, having the C_6F_5 group

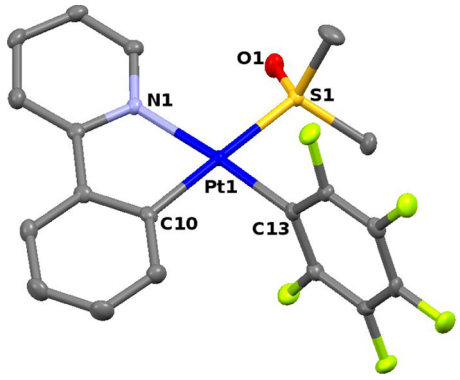

Figure 2. Molecular view of [Pt(C_6F_5)(ppy)(dmso)] (**2**).

dx.doi.org/10.1021/ic501458q | Inorg. Chem. 2014, 53, 8770–8785

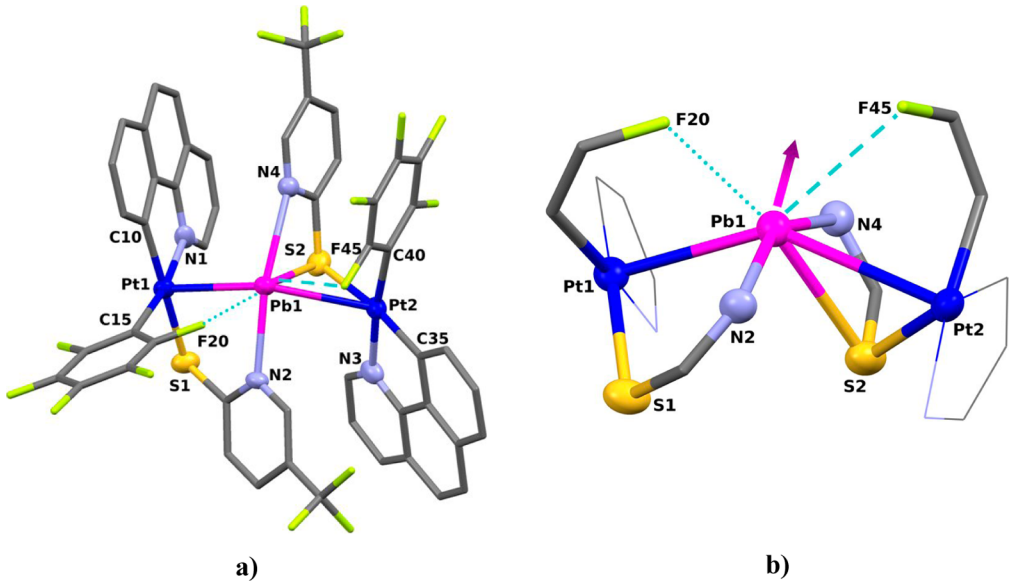

a) b)

Figure 3. (a) Drawing of the structure of **4**·0.9CH_2Cl_2 (orange crystals). (b) Detail of the environment of Pb^{II} (the arrow suggests the direction where the lone pair is located).

coordinated in a position *cis* to the metalated C(10) atom of the ppy ligand. The bond lengths and angles are not unusual,[19] and not unexpectedly, the complex crystallizes as head-to-tail dimers through moderate intermolecular interactions (3.270 Å) between the ppy ligands (Figure S3 (Supporting Information)).

As was previously communicated,[18] for complex **3** (see Chart 1) two different orange crystalline forms with distinct structural and emissive properties were obtained under different conditions: CH_2Cl_2/*n*-hexane for **3**·1.5CH_2Cl_2 or acetone/*n*-hexane for [**3·acetone**]·0.5acetone, denoted as **3** and **3·acetone**, respectively, hereafter. It was found that the incorporation of acetone (and likely also other specific VOCs) enforces a change from a local Pt_2N_2S (*trans-N,N*) to a more symmetric Pt_2N_2O (*cis-N,N*) coordination around the Pb^{II} with a concomitant and remarkable blue shift in the emission (620 nm for **3** to 580 nm for **3·acetone**).

In light of these results, similar crystallographic and luminescence studies were performed for the related clusters **4**–**6**. In the case of **4**, upon addition of 1 drop of acetone, not only a reversible change of the luminescence from orange-yellow to yellow-green but also a visual color change of the solid from orange to yellow was observed. Fortunately, two different crystal forms depending on the solvent could also be obtained. Crystallization of **4** from CH_2Cl_2/*n*-hexane at −30 °C produced orange crystals of [{Pt(C_6F_5)(bzq)}$_2$Pb(μ-SpyCF$_3$)$_2$]·0.9CH_2Cl_2 (**4**), whereas that from acetone/*n*-hexane afforded yellow crystals of [{Pt(C_6F_5)(bzq)}$_2$Pb(μ-SpyCF$_3$)$_2$(acetone)$_{1.5}$] (**4·(acetone)**$_{1.5}$). The structure of the orange form **4** resembles that of **3**[18] (Figure 3, Table 1 and Table S2 (Supporting Information)) with some differences in the bond lengths. It displays a bent Pt–Pb–Pt core (141.54(1)°) with a short Pt1–Pb bond (2.7774(4) Å), close to the sum of the covalent radii (2.75 Å), supported by a (μ-$\kappa N,S$) SpyCF$_3$ ligand and a longer bond (Pt2–Pb 3.0877(4) Å), associated with the second pyridinethiolate acting as a 6e (μ-$\kappa^3 N,S,S$) bridging group. These Pt–Pb bond lengths are slightly shorter than those found in **3** (2.7832(3), 3.1642(3) Å) and are within the range reported for systems containing Pt–Pb bonds.[14a,b,d–h,16,17] The Pb–N bonds are slightly more asymmetrical (Pb–N2 2.495(5) Å, Pb–N4 2.775(5) Å) than those seen in **3** (2.565(5), 2.683(5) Å), and the Pb–S2 distance is somewhat larger (2.821(2) Å in **4** vs 2.797(1) Å in **3**), but both of them can be compared to those reported for [Pb(SpyCF$_3$-3)$_2$].[20] The Pb–S1 distance is too long (3.633 Å) and is clearly out of the reported range (2.45–3.03 Å) for primary coordination spheres in aggregated and base-stabilized lead(II) thiolates.[21] The Pb center features a primary Pt_2N_2S strongly distorted square pyramidal five-coordination, with the Pt atoms and the N atoms (N2–Pb–N4 153.15(16)°) defining the basal position (Pt–Pb–$N_{pyridin}$ 81.27(12)–97.82(11)°) and the bridging S2 center located in a tilted apex due to the acute angles S2–Pb–Pt2 (48.01(4)°) and S2–Pb–N4 (56.31(4)°), respectively. The remarkable void in the opposite hemisphere is indicative of the stereochemical activity of the lone $6s^2$ pair on the lead center. However, as shown in Figure 3b, the environment of the lead is also supplemented by two secondary *intramolecular* interactions with two *o*-fluorine atoms, one from each C_6F_5 ligand (Pb–F20 2.876(6) Å, Pb–F45 3.058(4) Å).[22] These interactions are weak, but as noted before, they are reflected in CD_2Cl_2 solution at low temperature in the fluorine–lead coupling constants (through space). The presence of two secondary Pb··F_o interactions in **4** is in contrast with the observation of only one in **3** (Pb··F20 2.959(3) Å; Table 1). This feature could be associated with the lower basicity of the SpyCF$_3$-5 ligand in relation to the Spy in **3**, which is also reflected in the J_{Pb-F_o} value observed in solution (1594 Hz in **4** vs 1552 Hz in **3**). An inspection of related bond lengths and contacts around Pb^{II} suggests that lone pair activity is somewhat more pronounced in the direction where the contacting atoms are located farthest, N4 and F45 (Pb–N4 2.775(5) Å and Pb···F45 3.058(4) Å). Interestingly, an analysis of the extended packing reveals that the void space around the lead(II) seems to be reduced by the occurrence of a short *intermolecular* fluorine···fluorine contact between F_o atoms of two C_6F_5 (2.734(5) Å) rings of different Pt_2Pb clusters (Figure S4 (Supporting Information)). This F_o···F_o interaction forms dimers, which are further connected by *intermolecular* π···π interactions (3.387(10) Å bzq···bzq) and reinforced by F_o··H(bzq) interactions (2.426(5), 2.595(5) Å).

dx.doi.org/10.1021/ic501458q | *Inorg. Chem.* 2014, 53, 8770–8785

Table 1. Selected Distances (Å) and Angles (deg) of Complexes **3**·1.5CH_2Cl_2, **3**·acetone·0.5(acetone), **4**·0.9CH_2Cl_2, **4**·(acetone)$_{1.5}$, **5**·2$CHCl_3$, **6**·4C_6H_6, **6**·4$CHCl_3$, **6**·2CH_2Cl_2, and **6**·acetone

	Pt1–Pb1	Pt2–Pb1	Pb1–N2	Pb1–N4	Pb1–S1	Pb1–S2	Pb1–O	Pb1–F	Pt1–Pb1–Pt2	N2–Pb1–N4
3·1.5CH_2Cl_2	2.7832(3)	3.1642(3)	2.565(5)	2.683(5)		2.797(1)		Pb–F20 2.959(3)	140.75(1)	151.72(15)
3·acetone	2.9790(3)	2.8401(3)	2.497(4)	2.568(3)	3.186(1)		2.775(5)	Pb–F20 3.037(3)	133.29(1)	84.20(13)
4·0.9CH_2Cl_2	2.7774(4)	3.0877(4)	2.495(5)	2.775(5)		2.821(2)		Pb–F20 2.876(6), Pb–F45 3.058(4)	141.54(1)	153.15(16)
4·(acetone)$_{1.5}$										
A	2.8654(6)	3.0902(6)	2.676(9)	2.608(9)		2.968(3)	Pb–O1 2.791(11), Pb–O2 2.937(9)	Pb–F20 2.895(8)	146.88(2)	144.7(3)
B	2.8038(6)	3.1408(6)	2.634(9)	2.593(9)		2.872(3)	2.967	Pb′–F16′ 2.829(8), Pb′–F45′ 3.031(6)	149.64(2)	140.4(3)
5·2$CHCl_3$	2.8326(4)	2.8998(4)			2.767(2)	2.691(2)		Pb–F18 2.914(4), Pb–F40 2.874(6)	169.88(1)	
6·4C_6H_6		2.9469(1)		2.669(3)		2.957(1)		Pb–F18 2.997(2)	156.22(1)	155.47(14)
6·4$CHCl_3$		2.9222(4)		2.674(5)		3.024(2)		Pb–F18 3.075(3)	155.02(1)	154.2(2)
6·2CH_2Cl_2[a]	2.7840(5)	3.0596(5)	2.564(8)	2.679(7)		2.858(3)		Pb–F14 2.874(6), Pb–F37 3.191(5)	137.58(2)	159.9(3)
6·acetone	2.7863(2)	3.534	2.603(3)	2.566(3)		2.7728(8)	2.897	Pb–F14 2.912(2)	132.25	142.11(8)

[a]Data for one (Pb1) of the three molecules (see the Supporting Information for molecules associated with Pb2 and Pb3).

Unlike the local Pt_2N_2S (*trans-N,N*) to Pt_2N_2O (*cis-N,N*) local environment that was found for the bzq/Spy complex **3** upon incorporation of one molecule of acetone (**3** to **3**·**acetone**), the structure of the yellow form **4**·(**acetone**)$_{1.5}$ (Figure 4, Table 1, and Table S3 (Supporting Information)) revealed that the incorporation of molecules of acetone takes place with minor changes in the primary sphere of coordination of Pb^{II}. Interestingly, the crystals of **4**·(**acetone**)$_{1.5}$ ($P2_1$ space group) were found to contain two different molecules (labeled **A** and **B**) in the asymmetric unit having different and very weak Pb···O(acetone) secondary contacts within the van der Waals limit. Thus, while in the molecule **A** the lead is involved in two long Pb···acetone interactions (Pb···O 2.791(11) and 2.937(9) Å), retaining only one F_o contact (F20···Pb 2.895(8) Å), in molecule **B** the Pb atom interacts more weakly with only one acetone molecule (Pb′–O′ 2.967(8) Å), retaining the two F_o··· Pb secondary contacts (2.829(8), 3.031(6) Å) observed in **4**. Although the Pb··O distances are slightly longer than those reported for the upper range in the primary coordination sphere of Pb^{II} (2.70 Å),[15b] the presence of these contacts in **4**·(**acetone**)$_{1.5}$ provokes an increase in the Pb^{II} coordination number in relation to the unsolvated orange **4** (from 7 to 8), which is reflected in a less asymmetrical Pt_2N_2S local environment with bond lengths, on average, longer than those found in **4** (see Table 1). The more *holodirected* environment around the Pb in the acetone solvate **4**·(**acetone**)$_{1.5}$ is evidenced by the wider Pt–Pb–Pt angle (146.88(2)° (**A**), 149.64(2)° (**B**) in **4**·(**acetone**)$_{1.5}$ vs 141.54(1)° in **4**) and more symmetrical Pb–N distances, though the N–Pb–N angle observed in both molecules **A** and **B** is more acute (144.7(3) **A**, 140.4(3)° **B** vs 153.15(16)° in **4**). All of these structural details point to lower stereochemical activity of the lone pair in the yellow form **4**·(**acetone**)$_{1.5}$ in relation to the orange **4**. As it is illustrated in Figure 4, both molecules (**A** and **B**) are contacting through $\pi\cdots\pi$(bzq) and F_o·· H interactions involving one of the platinum fragments (Pt1, Pt1′). These intermolecular contacts are clearly weaker than those observed in **4** ($\pi\cdots\pi/F_o$··H 3.588(20)/2.509(7), 2.626(7) Å (**4**·(**acetone**)$_{1.5}$) vs 3.387(10)/2.426(3), 2.595(5) Å (**4**)). We hypothesize that not only the different coordination environment of the Pb center in both forms but also the packing changes play a role for the observed vapochromism and vapoluminescent behavior of this cluster.

In contrast to benzoquinolinyl clusters (**3** and **4**), the molecular structure of the orange ppy/Spy derivative **5** (crystallized as **5**·2$CHCl_3$; Figure 5, Table 1 and Table S4 (Supporting Information)) reveals the formation of a rather symmetrical and linear Pt_2Pb cluster (Pt–Pb–Pt 169.88(1)°), in which the N atoms of the μ-$\kappa N,S$-Spy ligands are surprisingly ligated to the platinum centers (Pt–N 2.148(5), 2.120(6) Å). The Pb center exhibits a primary "Pt_2S_2" four-coordination, with Pt–Pb (2.8326(4), 2.8998(4) Å) and Pb–S bonds shorter (2.691(2), 2.767(2) Å), on average, than those found in **3** and **4**, supplemented by two secondary Pb···F_o *intramolecular* interactions (2.874(6), 2.914(4) Å). The formally neutral Pb center acquires a final slightly distorted octahedral coordination, as evidenced by the angles (S–Pb–S and F–Pb–F ca. 96°) close to 90°, thus indicating that the stereochemical activity of the lone pair is negligible. This structural feature, together with the rather tight packing generated (Figure S5 (Supporting Information)), could explain the experimental observation that this cluster does not exhibit visual response (color or luminescence) to the vapor of donor solvents such as

dx.doi.org/10.1021/ic501458q | Inorg. Chem. 2014, 53, 8770–8785

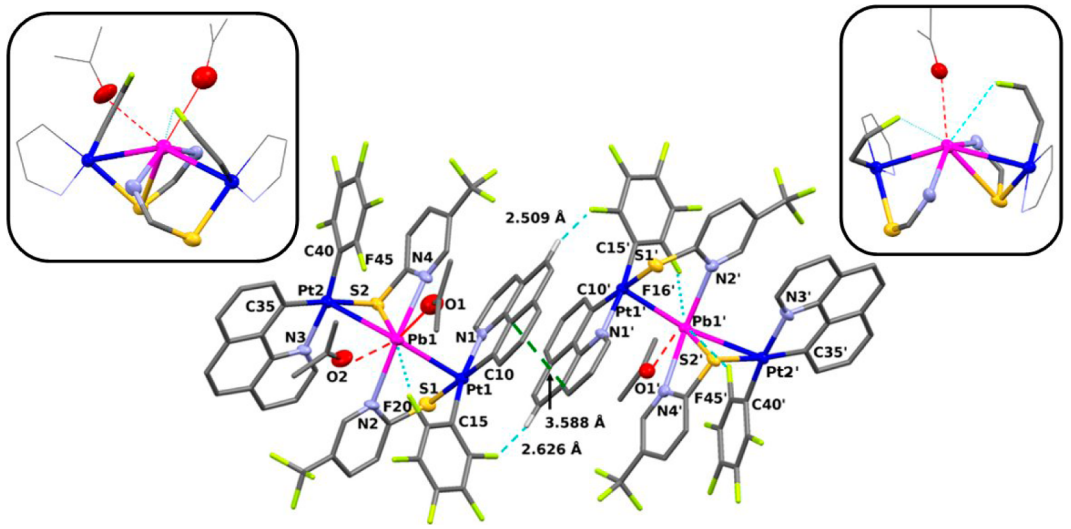

Figure 4. X-ray molecular structure of **4·(acetone)**$_{1.5}$ (yellow) showing the two types of molecules: (left) molecule **A** **4·(acetone)**$_2$ with its core (top left) and (right) molecule **B** of **4·(acetone)** with its core (top right). Intermolecular $\pi\cdots\pi$ (bzq···bzq) and $H_{bzq}\cdots F_o$ interactions between molecules **A** and **B** are also included.

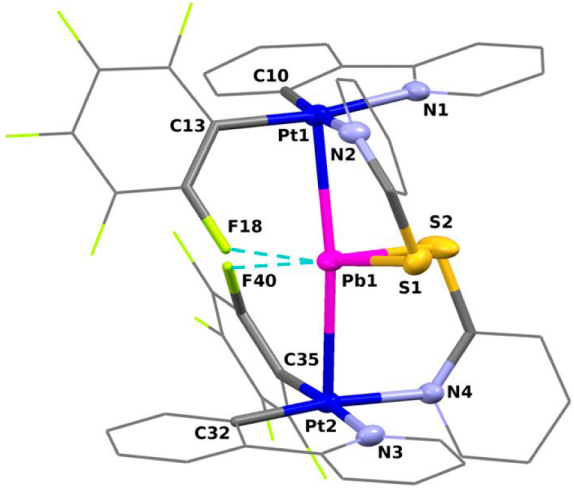

Figure 5. Molecular structure of **5**·2CHCl$_3$.

acetone, THF, and NCMe. In this complex the Pb is well embedded and, presumably, the activation energy to cause structural changes is higher than those required for **3** and **4**.

As **5**, the ppy/(SpyCF$_3$-5) complex **6**, isolated as a yellow solid by precipitation from a CH_2Cl_2 solution with *n*-hexane, did not showed visual changes to vapors. However, while exploring different crystallization conditions, we found that its color (yellow or orange) and luminescence (yellow or orange-red) depend on the solvent, concentration, and also the velocity of crystallization. Thus, slow crystallization from CH_2Cl_2, $CHCl_3$, or benzene always yielded yellow crystals. However, from very concentrated CH_2Cl_2 solution both yellow and dark orange crystals separated, whereas pale orange crystals were obtained from acetone (or acetone/hexane). In addition, we noted that fast evaporation of **6** to dryness in any of these solvents always generated an orange film with a very strong red luminescence. For cluster **6** we could crystallize four solvates that were subjected to X-ray crystallography (Table 1 and Tables S5−S10 (Supporting Information)): yellow crystals of stoichiometry **6**·4C$_6$H$_6$ and **6**·4CHCl$_3$ (hereafter **6-y**), pale orange crystals of the solvate [{Pt(C$_6$F$_5$)(ppy)}$_2$Pb(SpyCF$_3$)$_2$(acetone)] (**6·acetone**), and orange crystals by cooling a concentrated solution of CH_2Cl_2 (**6**·2CH_2Cl_2, denoted as **6-o**). The structures of the two yellow solvates are very similar (see Table 1 and Tables S6 and S7 (Supporting Information)) with only small differences in bond lengths and angles and clearly different from those of the orange crystals **6-o** and **6·acetone**. Selected molecular views of **6-y**, **6-o**, and **6·acetone** highlighting the central environment around the Pb^{II} center are shown in Figure 6, whereas complete structures are given in the Supporting Information (Figures S6−S11 and Tables S5−S10). The asymmetric unit of the orange crystals **6-o** is built from three rather similar molecules, and therefore, the data of only one of them are included in Table 1. The structural details are comparable to those of orange crystals of **3** and **4** obtained from CH_2Cl_2. The Pb^{II} center (Figure 6b) also features a primary "Pt$_2$N$_2$S" coordination with asymmetric Pt−Pb (2.7840(5), 3.0596(5) Å) and Pb−N (2.564(8), 2.679(7) Å) bond distances. Pb−S distances of 2.858(3) and 3.596(5) Å indicate that only one of the sulfur atoms takes part in the bonding, which is supplemented (up to 7), in the direction of the open void, by two long Pb−F_o contacts. The orientation of the Pt fragments (dihedral angle ∼64°) leads to a Pt−Pb−Pt angle (137.58(2)°) more acute than those seen in **3** and **4**, whereas N−Pb−N is more linear (∼160°). In the crystal, the molecules are arranged in a head to head manner through $\pi\cdots\pi$ interactions (ppy···ppy and C$_6$F$_5$····C$_6$F$_5$) of different degrees to form extended chains, which are additionally connected by extensive H···F contacts (see Figures S6 and S7).

In contrast, slow crystallization from benzene and $CHCl_3$ (and also from CH_2Cl_2) seems to allow a symmetrical coordination of both Pt units (dihedral angle ca. 67°) around Pb^{II} in the yellow forms (**6-y**; see Figure 6a for **6**·4CHCl$_3$), pointing to a lower stereochemical activity of the lone pair. In both yellow crystals, the Pb is coordinated to the two Pt and N atoms of both platinum units with identical Pt−Pb (∼2.95 Å in **6**·4C$_6$H$_6$, 2.92 Å in **6**·4CHCl$_3$) and Pb−N (∼2.67 Å) bond lengths, its formal coordination being increased (up to 8) with two clearly weaker Pb···S and Pb···F_o bonding interactions (Table 1). The Pb−S distances (2.957(1)−3.025(3) Å) are slightly larger than the shorter distances seen in **6-o** and bzq

dx.doi.org/10.1021/ic501458q | Inorg. Chem. 2014, 53, 8770−8785

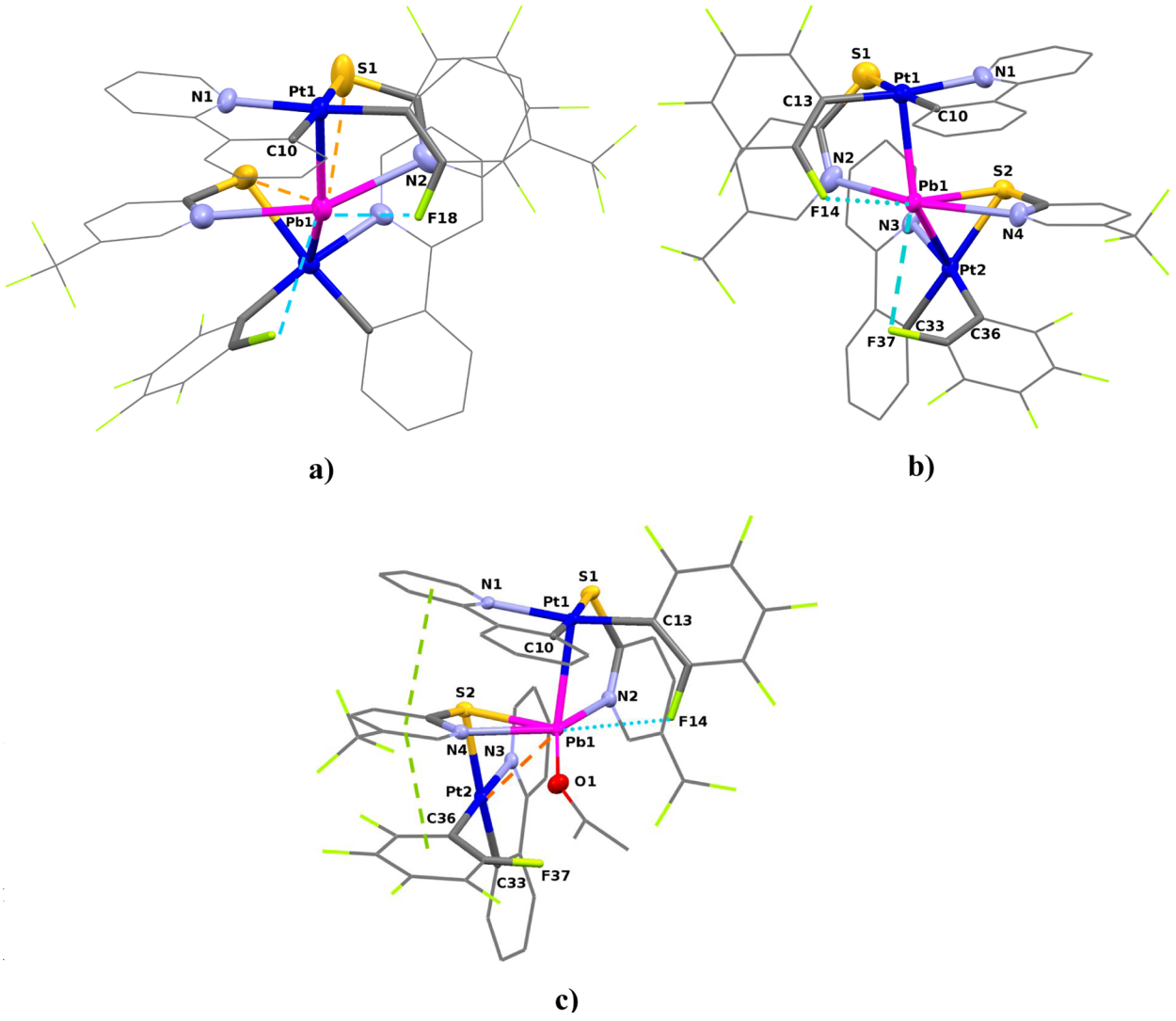

Figure 6. Molecular structures of (a) **6**·4$CHCl_3$ (**6-y**), (b) **6**·2CH_2Cl_2 (**6-o**), and (c) **6·acetone**.

clusters (**3** and **4**), suggesting that the coordination of the thiolate is somewhat midway between μ-κ^2N,S and μ-κ^3N,S,S. Interestingly, the Pt−Pb−Pt angle also increases in relation to that observed in **6-o**, being comparable to the angle N−Pb−N (~155, 154°). In the crystal the molecules also forms chains, but the main difference with the packing observed in **6-o** is that the neighboring molecules are associated in a face to face manner through the ppy ligands (3.346 Å (**6**·4$CHCl_3$), 3.689 Å (**6**·4C_6H_6)) (Figures S8−S10 (Supporting Information)).

Interestingly, crystallization from acetone enforces an essentially perpendicular disposition of both Pt units (dihedral angle 80.23°), provoking asymmetry greater than that observed in **6-o** and the presence of two very distinct Pt centers. In **6·acetone**, one of the Pt units is involved in a short Pt1−Pb bond (2.7863(2) Å) and the other in a weak contact (Pb−Pt2 3.534(1) Å) (Figure 6c). Similarly, one of the $SPyCF_3$-5 ligands chelates the Pb (Pb−S2/N4 2.7728(8)/2.566(3) Å) and is bonded to Pt2 (μ-κ^3N,S,S), whereas the other behaves as typical μ-κ^2N,S. The remaining closest donor atoms around the Pb are one F_o (2.912(2) Å) and the oxygen of the acetone (2.897(3) Å). The interaction with the solvent is very weak; consistent with this, the acetone molecules escape from the crystal in air, as confirmed by NMR spectroscopy. Interestingly, the conformation of the Pt coordination planes and the chelating thiolate bridge favors the presence of very close $\pi\cdots\pi$ *intramolecular* contacts (ppy···$SpyCF_3$···C_6F_5 3.240−3.443 Å), which likely also play an important role in the stabilization of this structure (Figure 6c). In addition, the trinuclear Pt_2Pb molecules are arranged so that the same ppy and C_6F_5 ligands are closely located in a head (ppy···ppy 3.345(5) Å) and tail (C_6F_5···C_6F_5 3.230(5) Å) fashion, giving rise to a columnar network (Figure S11 (Supporting Information)). This packing is somewhat comparable to that seen in **6-o** but is in contrast with those observed for the yellow forms (**6**·4C_6H_6 and **6**·4$CHCl_3$) mainly based in more tightly intermolecular $\pi\cdots\pi$ of ppy groups (Figures S8 and S10 (Supporting Information)).

Photophysical Properties. *[Pt(ppy)(C_6F_5)(dmso)] (**2**).* The precursor **2** shows intense absorptions (CH_2Cl_2) in the range 246−323 nm, attributable to metal perturbed $\pi\pi^*$ intraligand (^{1}IL, bzq, C_6F_5) transitions, and two additional less intense bands at 350 and 365 nm which, with reference to previous assignments,[19f,h] are attributed to an admixture of ^{1}IL and ^{1}MLCT (Table S11 (Supporting Information)). The low-energy absorption showed a remarkable solvent dependence, shifting to lower energies in acetone or 2-MeTHF, indicating that it possesses a significant charge-transfer character. Upon

dx.doi.org/10.1021/ic501458q | *Inorg. Chem.* 2014, 53, 8770−8785

Table 2. Photophysical Data for Complexes 2−6 in the Solid State at 298 and 77 K

compd	T/K	λ_{em} (nm)[a]	τ (μs)	ϕ[b]	k_r[c]	k_{nr}[d]
[Pt(C_6F_5)(ppy)(dmso)] (**2**)	298	490, 518_{max}	20.1	13	6.5×10^3	5.7×10^4
	77	500_{max}, 537	70.0			
[{Pt(C_6F_5)(bzq)}$_2$Pb(Spy)$_2$] (**3**)[18]	298	620	1.6	34	2.1×10^5	9.5×10^5
	77	620	5.2			
[{Pt(C_6F_5)(bzq)}$_2$Pb(SpyCF$_3$)$_2$] (**4**)	298	580	3.6 (18%), 0.5 (82%)	32.2	3.0×10^5	1.4×10^6
	77	570	9.8			
4-grinding	298	610	0.1 (47%), 0.5 (53%)	10.6	3.4×10^5	3.6×10^6
	77	600	7.1			
4-acetone	298	545	0.2 (24%), 0.4 (76%)	22.8	6.5×10^5	3.7×10^6
	77	535	11.5			
4-THF	298	575	0.2 (37%), 0.4 (63%)	12.4	3.8×10^5	3.5×10^6
	77	570	11.0			
4-MeOH	298	558	0.08(47%) 0.2 (53%)	8.6	6.0×10^5	7.6×10^6
	77	545	15.7			
4-MeCN	298	550	0.3 (27%) ,0.8 (73%)	29	4.4×10^5	2.1×10^6
	77	550	12.5			
4-C_6H_6	298	570	0.3 (57%), 0.7 (43%)	19.5	4.1×10^5	2.6×10^6
	77	570	10.4			
[{Pt(C_6F_5)(ppy)}$_2$Pb(Spy)$_2$] (**5**)	298	620	3.2 (13%), 0.6 (87%)	13.8	1.5×10^5	1.2×10^6
	77	616	7.2			
[{Pt(C_6F_5)(ppy)}$_2$Pb(SpyCF$_3$)$_2$] (**6**) yellow solid[e]	298	550	0.3 (24%), 0.9 (76%)	34.6	4.6×10^5	2.0×10^6
	77	550	11.7			
6-o (crystals)	298	610	1.24	14.0	1.1×10^5	9.4×10^5
	77	630	6.5			
6·acetone (crystals)	298	570	0.05 (34%), 0.58 (66%)	3.4	8.5×10^4	2.6×10^6
	77	550	12.9			
6 (red solid, fast precipitation from CH_2Cl_2)	298	660	0.4 (69%), 0.8 (31%)	39.6	7.6×10^5	3.2×10^6
	77	650	4.4			
6 (pale orange, fast precipitation from acetone)	298	630	0.08 (79%), 0.2 (21%)	24.5	2.3×10^6	1.3×10^7
	77	645	8.8			
6-grinding	298	600	0.1 (23%), 0.7 (77%)	5.2	9.3×10^4	1.9×10^6
	77	600	7.7			

[a] λ_{exc} for **2** 365 nm; λ_{exc} for **3**−**6** 395−500 nm. [b] In percent; determined by the absolute method using an integrated sphere. [c] $k_r = \phi/\tau_{average}$. [d] $k_{nr} = 1/\tau_{average}(1 - \phi)$. [e] From THF and CH_3CN weak emission centered at 580 and 600 nm, respectively.

photoexcitation, it displays a structured emission (CH_2Cl_2 484, 518, 555 nm), which has negligible solvent and concentration dependence and exhibits a slight rigidochromism at 77 K (Table S12 (Supporting Information)). In the solid state, the emission is somewhat broader, showing a slight red shift (Table 2; 490 nm at 298 K, 500 nm at 77 K), probably because of the short $\pi\cdots\pi$ intermolecular interactions, as observed by X-ray. The structuration and long lifetime (20.1 μs, 298 K) suggest a predominant ^{3}LC transition with some ^{3}MLCT (Table 2).

[{Pt(C$_6$F$_5$)(C^N)}$_2$Pb(μ-SpyR)$_2$]. Detailed data of the photophysical properties of the clusters **3**−**6** in solution and in the solid state are compiled in Tables S11 and S12 (Supporting Information) and Table 2.

Solution. Complexes **3**−**6** all exhibit rather similar UV−vis profiles in CH_2Cl_2 or acetone solutions. In particular, the formation of the clusters is characterized by the presence of two visible low-energy absorptions (with a shoulder at ca. 485 nm) in the range 390−485 nm tailing to 520−530 nm. According to TD-DFT calculations in the gas phase (**3**;[18] see below for **4** and **6**), these transitions mainly could be ascribed to admixtures of thiolate-to-cluster ^{1}[(SpyR) → Pb,Pt] ^{1}L′CCT and ^{1}L′LCT (SpyR → C^N) charge transfer with some ^{1}MM′CT contribution. In agreement with this assignment, no noticeable changes were observed from the bzq (**3**/**4**) to the ppy (**5**/**6**) complexes and only minor blue shifts were detected from the Spy to the SpyCF$_3$ species (see Table S11 and Figure S12 (Supporting Information) for **5** and **6**).

Upon photoexcitation into the low-energy bands (395−500 nm), the complexes displays a broad featureless weak emission centered at 620 nm for the Spy derivatives (**3**, **5**) that is slightly blue-shifted for SpyCF$_3$ complexes (600 nm (**4**), 610 nm (**6**)) in fluid CH_2Cl_2 solution. In acetone solution, the emission is weaker but the maxima, clearly measured at higher concentration (10^{-3} M), remain essentially unchanged (see Table S12 (Supporting Information)). This emission can be attributed to phosphorescence ligand to cluster ^{3}L′CCT [(SpyR) → Pb,Pt] with some ^{3}MM′CT (M = Pt, M′ = Pb) and ^{3}L′LCT (SpyR → C^N) character, as supported by TD-DFT studies. When the temperature is lowered to 77 K, the intensity of the emissions increases remarkably. Curiously, whereas the Spy-bridged complexes displayed only one band with a remarkable (570 nm (**3**)) or slight (600 nm (**5**)) rigidochromism in CH_2Cl_2 glasses, several bands were observed for the SpyCF$_3$ derivatives (555, 645_{max}, 730 nm (**4**), 540, 640_{max}, 720 nm (**6**); Figure S13 (Supporting Information)). These bands are related to different excitation profiles, suggesting the presence of different emissive manifolds. It is likely that the main band and the small high-energy component originate from two different conformations of the pyridinethiolate−Pt fragments around the Pb^{II} formed in the freezing process, while the low-energy manifold (720−730

dx.doi.org/10.1021/ic501458q | Inorg. Chem. 2014, 53, 8770−8785

nm) could be ascribed to excimers or aggregates ($\pi\cdots\pi$ or Pt··Pt), which are well-known in Pt^{II} cycloplatinate complexes. In acetone glasses, the emission maximum of **3** is also blue-shifted (570 nm), whereas those of **4** and **6** are similar to those observed in fluid solution (600 (**4**), 595 nm (**6**)). In complex **5** two emission bands (575, 620 nm), probably related to two different conformers, were observed.

Solid State. The photophysical characteristics in solid state are compiled in Table 2 (Table S11 (Supporting Information) for reflectance), and illustrative examples are given in Figures 7

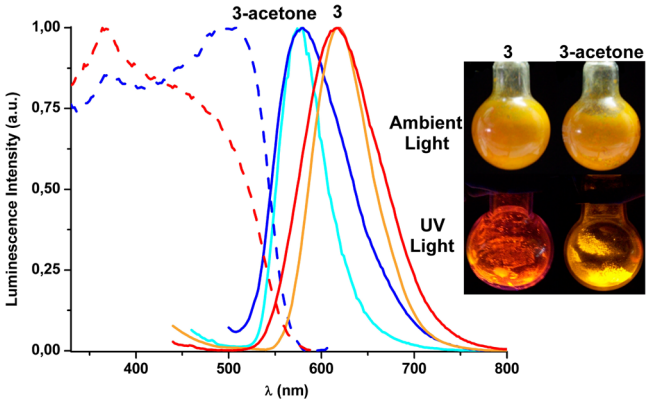

Figure 7. Normalized excitation (dotted lines) and emission (solid lines) of **3** and **3-acetone** in the solid state at 298 K (red and deep blue) and at 77 K (orange and light blue). Photographs show the color and luminescence changes of **3** after addition of 1 drop of acetone.

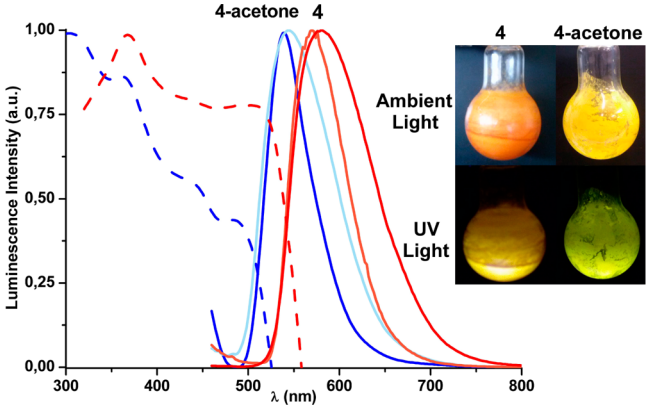

Figure 8. Normalized excitation (dotted lines) and emission (solid lines) spectra of **4** and **4-acetone** (powders) at 298 K (red and deep blue) and at 77 K (orange and light blue). Photographs show the color and luminescence changes of **4** after addition of 1 drop of acetone.

and 8 and in the Supporting Information (Figures S14–S19). We note that the as-obtained solids (orange **3**–**5** and yellow **6**) are free of solvent, as confirmed by NMR spectroscopy. They are characterized by broad low-energy absorptions (400–490 nm) tailing to ca. 530 nm (**6**) or 560 nm (**3**–**5**), which are ascribed to mixed ^{1}L′CCT [(SpyR) → Pb,Pt]/^{1}L′LCT (thiolate → C^N) transitions, to which additional contribution from extensive $\pi\cdots\pi$ contacts (as supported by X-ray) cannot be discarded.

Under irradiation (λ_{ex} 395–500 nm) the as-synthesized solids display a bright orange (620 nm (**3**, **5**); 580 nm (**4**)) or yellow (550 nm (**6**)) emission, whose maxima remain essentially unchanged at 77 K (Figures 7 and 8 and Figure S16 (Supporting Information)). The lifetimes are in the microsecond domain, implying a triplet excited state with phosphorescence character, and increase remarkably at 77 K, likely due to suppression of thermally activated nonradiative processes. We noted that for **4**–**6**, at room temperature, the emission decays were best fitted with two components, which might be attributed to small different structural environments, as was recently shown by Coppens in copper complexes.[23] The observed blue shift in complexes **4** and **6** can be attributed to the lower donor character of the $SpyCF_3$ ligand, supporting a significant ^{3}L′CCT character for the emission.

Vapochromism and Mechanochromism Properties. As mentioned in the Introduction, the flexibility of coordination of Pb allows it to modify its coordination through tuning the degree of stereochemical activity of the lone pair, which seems to be decisive in the observed vapochromic behavior of the bzq complexes **3** and **4** and in the mechanochromism of **4** and **6**. As noted before, in the case of complex solid **5**, its exposure to vapors or a drop of solvents of different VOCs has no visual effect in the color or emission. This behavior could be related to the rather stable octahedral geometry around the formally neutral Pb^{II} center with the Spy acting as a symmetrical μ-κ^2N(Pt),S(Pb) species.

As was previously communicated,[18] the as-obtained powder bzq/Spy complex **3** shows the same color (orange) as in the crystalline forms (**3**·1.5CH_2Cl_2) and the acetone adduct **3-acetone**, but its emission is different (Chart 1, Figure 7). Thus, **3** (powder or crystalline) displays a bright orange-red luminescence centered at 620 nm (ϕ = 0.34), whereas the acetone form **3-acetone** emits at 580 nm (yellow-orange, ϕ = 0.14). At 77 K, the bands narrow but the maxima do not change. Interestingly, as is seen in Figure 7, both **3** and **3-acetone** display similar excitation spectra, which suggests that the blue shift in the emission of **3-acetone** in relation to that of **3** could be related to a smaller Stokes shift in the acetone solvate (4593 cm^{-1} (**3**) vs 3231 cm^{-1} (**3-acetone**)). A similar emission change was found when solid **3** was exposed to Me_2CO vapor, and the specific response to other donor solvents such as MeCN, MeOH, and THF was described. DFT calculations indicated that the distortion in the *hemidirected* form **3** is notably reduced (less p character for the lone pair of Pb^{II}) upon excitation, whereas in the more *holodirected* solvate structure **3-acetone** these changes are negligible. Thus, the change in the emission color upon uptake of VOCs can be primarily attributed to a different distortion of the geometry around the Pb^{II} center upon photoexcitation. In contrast, as commented before, color and luminescence changes were observed for **4** (powder and crystalline) and the acetone solvate **4**·(**acetone**)$_{1.5}$. Thus, when **4** was treated with 1 drop of acetone, a color change occurred from orange to yellow under ambient light and the bright yellow-orange luminescence turned to yellow-green under UV light (Figure 8). This behavior, visible to the naked eye, is reflected in a slight blue shift in the diffuse reflectance spectra (Figure S14 (Supporting Information)) and in the corresponding emission spectra. As is illustrated in Figure 8, a significant blue shift from 580 to 545 nm is observed in the emission at 298 K, which is slightly blue shifted at 77 K (535 nm). In contrast to the bzq/Spy complex (**3**), in this case **4** and **4**·(**acetone**)$_{1.5}$ display different excitation spectra, giving rise to similar Stokes shifts. Considering the increase in the Pb coordination due to weak contacts to the acetone molecules and the larger $\pi\cdots\pi$ stacking observed in the

dx.doi.org/10.1021/ic501458q | Inorg. Chem. 2014, 53, 8770–8785

XRD of **4·(acetone)**$_{1.5}$, these changes are attributed to the concomitant result of both effects. Interaction with the solvent molecules likely somewhat decreases the electrophilicity of the lead center, increasing the energy of the LUMO and the gap of the transition.

Similar response in color and luminescence was observed when solid **4** was exposed to acetone vapors at 298 K for a few minutes (~15 min), indicating that the transformation of **4** to **4-acetone** (likely similar to **4·(acetone)**$_{1.5}$) has occurred. On standing, the acetone was completely lost in ~12 h, with recovery of **4**. Desolvation by passing of a stream of air onto the sample of **4-acetone**, monitored using emission spectroscopy (Figure S17 (Supporting Information)), showed a gradual change from **4-acetone** to **4**; therefore, we cannot discard the formation of intermediate species. The response to other vapors was also examined (Figure S18 (Supporting Information) at 298 K and Table 2). Moderate and relatively fast color and emission changes were also observed with MeCN and MeOH (MeCN (~15 min) > MeOH (20 min)). Only minor changes were detected in the emission maxima upon sorption of THF and benzene after prolonged exposure (45 min for THF, C_6H_6), but the quantum efficiencies and the measured lifetimes decrease significantly, pointing to the occurrence of structural modifications (probably through the packing), which have a negative impact on the emission. Poor solvents such as *n*-hexane and diethyl ether, however, did not trigger a response. It is reasonable to conclude that the donor solvents (acetone, NCMe, MeOH) and probably also THF are able to contact the Pb^{II} center in a way similar to that described for **4·(acetone)**$_{1.5}$, provoking an increase in the Pb^{II} coordination number (more *holodirected* Pb^{II} environment) and changes in the packing, explaining the different emission observed. In any case, the vapor-induced responses are slightly smaller than those reported for the system **3**/**3-solvent**, for which a change from a local Pt_2N_2S environment (*trans-N,N*) to Pt_2N_2O (*cis-N,N*) around the Pb^{II} was confirmed by XRD.[18] We also observed that the color and the emission of **4** are slightly red-shifted by crushing the solid in a ceramic mortar (see Table 2).

As noted before, the color and emission characteristics of the ppy/SpyCF$_3$ complex **6** are significantly altered depending on the crystallization conditions (see Figure S15 (Supporting Information) for reflectance). The yellow microcrystalline solid **6-y** displays an intense yellow emission (550 nm, ϕ = 34.6%), while dried pale orange crystals prepared from acetone (**6·acetone** form) exhibit a weaker yellow-orange emission (570 nm, ϕ = 3.4%) and the orange crystals **6-o** (from concentrated CH_2Cl_2 solution) emit at 610 nm (ϕ = 14%) (Table 2, Figure S19 (Supporting Information)). The notable red shift of the orange forms could be mainly ascribed to the presence of one very short Pt–Pb bond (~2.78 Å) in the orange forms **6-o** and **6·acetone** vs ~2.95 Å in the yellow **6**·4C_6H_6 and 2.92 Å in **6**·4$CHCl_3$. The relatively strong *intramolecular* (in **6·acetone**) and *intermolecular* $\pi\cdot\cdot\pi$ interactions (in both orange forms) presumably also reduce the gap of the transition and favor exciton coupling. As seen in Figure 6, these forms (**6-o** and **6·acetone**) are generated by the twisting of the second platinum fragment associated with the μ-κ^3N,S,S bridging ligand around the lead center, which closes the Pt–Pb–Pt angle by ca. 20° in relation to that of **6-y** and seems to be favored in acetone solution or under kinetic conditions by quick precipitation from different solvents. The remarkable structural difference between the yellow forms **6-y** and **6-o** could explain the inability of acetone and other solvent vapors to promote the change, which is, however, observed by dissolving the yellow solid in the corresponding solvent. Thus, although the examined solvent vapors (NCMe, THF, acetone, benzene, ...) have no visual change on the yellow solid **6**, the emissions of the solids (from pale orange to orange-red) obtained by fast precipitation after dissolution of **6** in different solvents range from 580 nm in THF to 660 nm in CH_2Cl_2 (Figure 9). Interestingly, we also

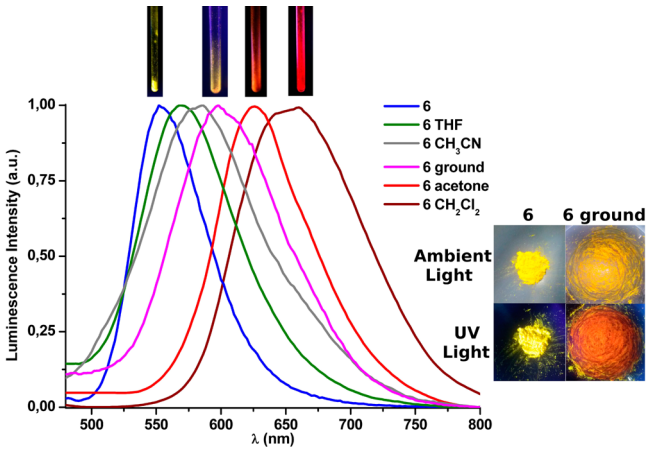

Figure 9. Normalized emission spectra of the unground yellow solid **6**, **6-ground**, and those solids obtained (orange-red) by evaporation of the appropriate solution of complex **6** in different solvents. Photographs show the color and the luminescence change of **6** after grinding.

found that the initial yellow form was easily recovered by stirring the orange or orange-red solids in *n*-hexane for ca. 2 h. By heating the red solid obtained from CH_2Cl_2 at ca. 80 °C, its color slowly blue-shifted, yielding a final pale orange after 24 h. These facts suggest that fast crystallizations probably give rise to structures with low-symmetry environments at Pb and short Pt–Pb distances, which slowly undergo conformational switching to more symmetrical and stable structures by stirring in hexane or prolonged heating.

We also found that this cluster exhibited notable *mechanochromic* behavior, which is illustrated in Figure 9. Thus, after the yellow solid was ground, the resulting orange powder showed a red shift in its absorption (Figure S15 (Supporting Information)) and emission spectra (λ_{max} 600 nm) with a remarkable decrease in its quantum yield (ϕ = 5.2). The remarkable red shift in the crushed powder suggests that, after grinding, some clusters could present an asymmetric structure (similar to **6-o** or **6·acetone**) with one very short Pt–Pb bond and close $\pi\cdots\pi$ stacking interactions. This behavior is not surprising, as most of the *mechanochromic* luminescent transition-metal complexes are related to modulation of metallophilic interactions, and is further support of the influence of the Pt–Pb bond in the excited state.

Computational Studies. To gain some insight into the photophysics of these complexes, we performed theoretical calculations in the gas phase for the solvent-free clusters **4** and **6** and for the two solvate molecules **4·(acetone)**$_2$ and **6·acetone**. The S_0 and T_1 state geometries were optimized at the B3LYP/LanL2DZ(Pt and Pb)/6-31G**(ligand atoms) level. The most important geometrical parameters (bond lengths and angles) are given in Table S13 of the Supporting Information. Detailed orbital compositions and electron-density contours are

dx.doi.org/10.1021/ic501458q | Inorg. Chem. 2014, 53, 8770–8785

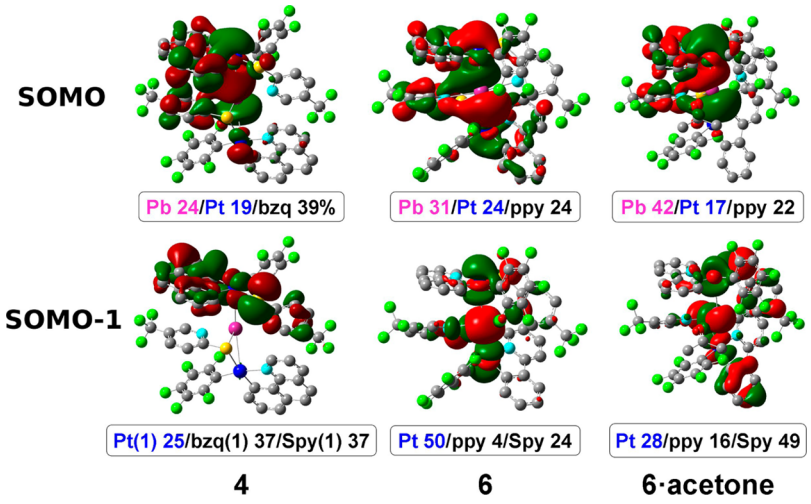

Figure 10. SOMO and SOMO-1 of complexes **4**, **6**, and **6·acetone**.

detailed in Tables S14 and S15 and Figures S20–S22 (Supporting Information).

The calculations (state S_0) agree reasonably well with the geometrical parameters obtained in the X-ray structures for all complexes except for **4**·(**acetone**)$_2$. Thus, for complexes **4** and **6·acetone**, calculations reproduce the asymmetric Pt–Pb distances, although in both complexes the short distance fits better that the long distance (Pt–Pb experimental 2.7774(4), 3.0877(4) Å vs calculated 2.832, 3.507 Å for **4**). It should be noted that the B3LYP functional tends to overestimate bond lengths. Interestingly, the free solvent optimized structure for complex **6** is essentially symmetrical and reproduces the structural data found for the symmetrical yellow forms **6-y** obtained in benzene (**6**·4C_6H_6) and chloroform (**6**·4$CHCl_3$) or by slow crystallization (experimental 2.9222(4) Å vs calculated 2.920, 2.922 Å; see Table S13 (Supporting Information)), thus supporting the thermodynamic stability of this conformation. In the case of model complex **4**·(**acetone**)$_{1.5}$, the obtained S_0 geometry does not reproduce the X-ray geometry, showing remarkably larger Pt–Pb distances (2.8654(6), 3.092(6) Å vs calculated 3.709, 3.710 Å) and a wider Pt–Pb–Pt angle (146.88(2)° vs 179.71°) and, in contrast, relatively shorter Pb–N and Pb–S bond lengths (see Table S13). Therefore, TD-DFT and energy emission calculations were carried out only for **4**, **6**, and **6·acetone**.

The study of the composition of frontier molecular orbitals in terms of ligands and metals (Table S14 (Supporting Information)) of complex **4** shows that the HOMO and HOMO-1 are mainly located on Pt(2)/bzq(2) and Pt(1)/bzq(1)/Spy(1), respectively, while the LUMO has contribution from the metals associated with the short Pb–Pt bond and the corresponding bzq ligand (Pb 18%, Pt(1) 12%, bzq(1) 54%). For the symmetrical **6** and asymmetrical **6·acetone**, the composition of the frontier molecular orbitals is very different, despite the almost negligible contribution of the acetone molecule in **6·acetone**. Thus, for complex **6** having a symmetrical conformation, the HOMO and HOMO-1 are well distributed along both Pt units and the two bridging pyridinethiolate groups, with a large contribution of the latter (e.g., HOMO: Spy 51%, Pt 22%, ppy 25%), and the LUMO is mainly contributed from the Pb and the two Pt fragments (Pb 15%, Pt(1,2) 18%, ppy 53%) having Pt–Pb–Pt bonding character. In contrast, in **6·acetone** while the HOMO is located on the pending Pt unit (Pt(2) 38%, ppy(2) 50%), the HOMO-1 is mainly derived from the Spy bridging group associated with the short Pt(1)–Pb bond (Pt(1) 9% Spy(1) 83%). In this solvate the LUMO has the highest heterometallic contribution, being located on the short Pb–Pt(1) bond (Pb 24%, Pt 15%), also having bonding character, and the associated ppy(1) ligand.

Time-dependent (TD-DFT) calculations (Table S16 (Supporting Information)) in the gas phase show that the lowest calculated energy absorptions (446 nm (**4**), 424 nm (**6**), 460, 463 nm (**6·acetone**)) are in agreement with the trend observed experimentally (484 nm (**4**), 442 nm (**6-y**), 500 nm (**6·acetone**)) in the solid state. For complex **4**, the lowest energy transition is rather similar to that previously reported for **3**.[18] According to TD-DFT calculations (Table S16) it is assigned to a HOMO-1 (85%) + HOMO (11%) to LUMO transition having, therefore, strong contribution from the Spy-*κS,N* short-bonded [bzqPt](1)–Pb fragment and a minor contribution of the second [bzqPt](2). This transition mainly moves electron density from the thiolate-*κS,N* ligand to the Pb–Pt bond/bzq, being ascribed to ^{1}L′CCT/^{1}L′LCT admixture ^{1}[Spy → Pb,Pt(bzq)], somewhat perturbed by CT from the second Pt(bzq) (^{1}MM′CT).

In the symmetrical complex **6** (yellow form), the lowest electronic transition computed (HOMO-1 to LUMO) mainly transfers charge from both Spy ligands and the Pt atoms to the two Pt–Pb bonds in the Pt_2Pb unit and ppy coligands, also being identified as ^{1}L′CCT/^{1}L′LCT ^{1}[Spy → Pb,Pt(ppy)]. As far as the solvate **6·acetone** is concerned, the lowest transition calculated at 463 nm (HOMO to LUMO) has a remarkable charge transfer from the pendant [(ppy)Pt](2) unit to the short Pb–Pt(1) bond and the ppy(1) coligand, mainly being ascribed to metal–metal charge transfer (^{1}MM′CT) mixed with ^{1}LLCT (ppy to ppy). This transition lies very close to the next one (460 nm), which has, however, strong thiolate-to-cluster ^{1}[Spy → Pb,Pt1] charge transfer.

Details of the optimized triplet state geometries for the three complexes are collected in Table S13 (Supporting Information). The behavior of complex **4** resembles that previously found for **3**, and upon photoexcitation, **4** also rearranges to a geometry more symmetric than that calculated for the ground state with similar Pt–Pb lengths (3.101, 3.166 Å T_1 vs 2.832, 3.507 Å S_0). The triplet state geometry of **6** displays a

dx.doi.org/10.1021/ic501458q | Inorg. Chem. 2014, 53, 8770–8785

symmetrical environment around Pb, with small changes in the Pt−Pb distances (2.793, 2.906 Å T_1 vs 2.920, 2.922 Å S_0) relative to S_0. Notably, the Pt−Pb−Pb angle opens from 146.30° in S_0 to 166.91° in T_1, reflecting the role of the trimetallic unit in the excited state. In the corresponding optimized T_1 state of **6·acetone**, the most relevant feature is the significant withdrawal of the pendant Pt(2) fragment (Pt−Pb distances 2.883, 4.393 T_1 vs 2.842, 3.858 Å S_0), which is compensated by the approach of the acetone molecule (2.683 T_1 vs 2.961 Å S_0). As seen in Figure 10 for **4**, **6**, and **6·acetone**, the singly occupied orbitals are distributed throughout the cluster with a high contribution of the metallic core (e.g., SOMO: Pb 24%, Pt 19% (**4**); Pb 31%, Pt 24% (**6**); Pb 42%, Pt 17% (**6·acetone**); Table S15 (Supporting Information)). It is worth noting that the contribution of the Spy ligands in all the computed SOMO-1s (37% (**4**) 24% (**6**) 49% (**6·acetone**)) is in agreement with the different emission energies observed in complexes **4** and **6**. The very asymmetric geometry calculated for **6·acetone**, in both S_0 and T_1, is reflected in the asymmetrical contribution of both Pt fragments with a negligible contribution of the pendant [(ppy)Pt](2) in the excited state. The shorter Pt−Pb distance in **6·acetone** relative to that in **6** and greater metallic contribution (55% (**6**) vs 59% (**6·acetone**)) is in line with the red shift observed in the emission of the solvate complex. The calculated emission energy, as the difference between the energy of T_1 and the energy of the singlet state with the optimized triplet state (at 568 nm for **4**, 537 nm for **6**, and 547 nm for **6·acetone**) agree qualitatively with the experimental data (580 nm for **4**, 550 nm for **6**, and 570 nm for **6·acetone**), supporting a ligand-to-cluster ^{3}L′CCT [Spy → Pt,Pb] excited state with some ^{3}MM′CT and ^{3}L′LCT (Spy to C^N) character.

CONCLUSIONS

In summary, we have prepared two distinct types of the Pt_2Pb clusters $[\{Pt(C_6F_5)(C\hat{}N)\}_2Pb(SpyR\text{-}5)_2]$ (**3**−**6**) and studied in detail their structures and photophysical properties. In spite of the fact that all clusters feature two Pt−Pb bonds supported by two bridging pyridine-2-thiolate ligands, the notable differences in the Pb environment and, consequently, in the stereochemical activity of the $6s^2$ lone pair strongly affects their photophysical response. It was found that only the presence of *asymmetric* (*hemidirected*) environments around the Pb^{II} seems to provoke stimulus-responsive luminescent behavior. Thus, the ppy/Spy cluster (**5**), formed by coordination of the pyridine-N atoms to the Pt center, displays a *symmetrical* "PbS_2Pt_2" core and exhibits a strong emission (mainly ^{3}L′CCT in nature), which is not sensitive to external stimuli. However, clusters **3**, **4** (bzq), and **6** (ppy, $SpyCF_3$), formed by a formal thiolate S-transfer from Pb^{II} to Pt^{II}, show an asymmetrical coordination around the formally charged Pb^{II} and are sensible to external stimuli. In **3** and **4** (bzq), the Pb^{II} exhibits an *asymmetric* "Pt_2N_2S" (*trans-N,N*) environment which changes to a more *symmetric* environment in their acetone adducts ("Pt_2N_2O" (*cis-N,N*) in **3·acetone** or "$Pt_2N_2SO_2$"/"Pt_2N_2SO" in **4·(acetone)$_{1.5}$**), provoking a significant and reversible blue shift vapoluminescence response (also vapochromic in **3**) from the bright orange emission of the as-obtained solids (^{3}L′CCT with some ^{3}MM′CT and ^{3}L′LCT (SpyR → C^N) character), upon exposure to donor solvents. In the case of **3**, TD-DFT calculations suggest that the change in emission color is related to a smaller Stokes shift (in **3·acetone**), attributed to a different distortion of the geometry (in **3** and in **3·acetone**) around the Pb^{II} center upon photoexcitation. However, in the system **4**, in which both forms show similar Stokes shifts, these changes are attributed to the concomitant effect of a more *holodirected* Pb environment and larger $\pi\cdots\pi$ stacking in the acetone form.

For **6** (ppy/Spy-CF_3), three forms having different environments around the Pb^{II} ion and, hence, different emissions were found, depending on the solvent and crystallization conditions. In most of the solvents (CH_2Cl_2, $CHCl_3$, C_6H_6) slow crystallization generates a yellow form (**6-y**) with a primary *symmetrical* "Pt_2N_2" environment, supplemented up to 8 with weak contacts to the S and F_o, which displays an intense yellow emission. Fast crystallization from CH_2Cl_2 (or concentrated solution) gives rise to orange (**6-o**) or pale orange (**6·acetone**) crystals with a very *asymmetric* primary ("Pt_2N_2S" (**6-o**), "PtN_2S" (**6·acetone**)) coordination, supplemented by weak contacts (two $F_{o\ for}$ **6-o**; one F_o and O for **6·acetone**). In these colored forms, the most distinct feature is the twisting of one of the Pt units, shortening one of the Pt−Pb bonds to ∼2.78 Å. Curiously, in contrast with the behavior of the bzq clusters (**3** and **4**), in the solvate **6·acetone** the binding of acetone entails the *greatest asymmetry* (with a perpendicular orientation of the Pt fragments), which provokes the rupture of one of the Pt−Pb bonds that, in turn, is compensated by the presence of strong $\pi\cdots\pi$ *intramolecular* interactions. The lack of vapoluminescent response to vapor donor solvents (and even a drop of solvent) of the yellow solid **6** may be attributed to the marked structural differences between the yellow and solvate **6·acetone** forms, which makes its transformation difficult in rigid media. In fact, the more *symmetrical* and *holodirected* coordination at Pb^{II} (yellow form) seems to be the most thermodynamically stable form, as it is generated from the orange forms by stirring in hexane (sonication or prolonged heating). Theoretical calculations of **6** and **6·acetone** reproduce the observed *symmetrical* (**6**) and *asymmetrical* (**6·acetone**) environments around Pb and the energy of the emissions, supporting a ligand-to-cluster ^{3}L′CCT [SpyR → Pb,Pt] state with some ^{3}MM′CT and ^{3}LLCT character. Notably, the amorphous solids generated upon dissolution/evaporation of **6** in different solvents exhibit intense emission in a wide range from 580 nm (THF) to 660 nm (CH_2Cl_2) (depending on the solvent), a feature which is ascribed to the formation of metastable kinetic forms, presumably having an *asymmetric* environment at Pb and a short Pt−Pb bond. The yellow solid also shows *mechanochromic* behavior, with a remarkable red shift in color and luminescence upon grinding, which is ascribed to the transformation of the *symmetrical* form to more *asymmetrical* structures (similar to **6-o** or **6·acetone**) by mechanical stimuli. This work clearly demonstrates that, in these Pt_2Pb clusters, the different multistimulus-responsive luminescence and color switches are related to the versatility of the coordination of the Pb^{II} center, perturbed by $\pi\cdots\pi$ staking interactions, thus providing a relevant contribution to fields related to solid-state emission.

EXPERIMENTAL SECTION

Materials and Methods. All reactions were carried out under an argon atmosphere using standard Schlenk techniques and solvents from a solvent purification system (MBRAUN MB SPS-800). Elemental analyses were carried out with a Carlo Erba EA1110 CHNS/O microanalyzer. Mass spectra were recorded on a Microflex MALDI-TOF Bruker (MALDI) spectrometer operating in the linear and reflector modes with dithranol as the matrix. IR spectra were recorded on a Nicolet Nexus FT-IR spectrometer from Nujol mulls between polyethylene sheets. NMR spectra were recorded on Bruker

dx.doi.org/10.1021/ic501458q | Inorg. Chem. 2014, 53, 8770−8785

ARX 300 and ARX 400 spectrometers at 298 K. Chemical shifts are reported in parts per million (ppm) relative to external standards ($SiMe_4$ for ^1H and $CFCl_3$ for $^{13}C\{^1H\}$), and all coupling constants are given in hertz (Hz). The UV−vis absorption spectra were measured with a Hewlett-Packard 8453 spectrophotometer. Diffuse reflectance UV−vis (DRUV) data of pressed powders were recorded on a Shimadzu instrument (UV-3600 spectrophotometer with a Harrick Praying Mantis accessory) and recalculated with the Kubelka−Munk function. Excitation and emission spectra were obtained in a Jobin-Yvon Horiba Fluorolog 3-11 Tau-3 spectrofluorimeter. The lifetime measurements were performed with a Jobin Yvon Horiba Fluorolog operating in the phosphorimeter mode (with an F1-1029 lifetime emission PMT assembly, using a 450 W Xe lamp) or with a Datastation HUB-B with a nanoLED controller and software DAS6. The nanoLEDs employed for lifetime measurements were of wavelength 450 nm with pulse lengths of 0.8−1.4 ns. The lifetime data were fitted using the Jobin-Yvon software package. The complexes *cis*-$[Pt(C_6F_5)_2(dmso)_2]$,[19g] $[Pb(Spy)_2]$,[20] $[Pb(SpyCF_3\text{-}5)_2]$,[20] $[Pt(C_6F_5)(bzq)(acetone)]$ (**1**),[19a] and $[\{Pt(C_6F_5)(bzq)\}_2Pb(SpyCF_3)_2]$, (**3**)[18] were prepared as reported in the literature. Additional data for $[\{Pt(C_6F_5)(bzq)\}_2Pb(\mu\text{-}Spy)_2]$ (**3**): ^{19}F NMR (δ, 376.5 MHz, 186 K, CD_2Cl_2) −116.3 (t, $^3J_{Pt-F}$ = 405, 2 *o*-F), −123.5 (t, $^3J_{Pt-F}$ = 303, J_{Pb-F} = 1564, 2 *o*-F), −163.4 (t, 2 *p*-F), −163.5 (m_{br}, 2 *m*-F), −164.1 (m_{br}, 2 *m*-F).

Preparation of $[Pt(C_6F_5)(ppy)(dmso)]$ (2). 2-Phenylpyridine (0.23 gr, 1.46 mmol) was added to a toluene solution (20 mL) of *cis*-$[Pt(C_6F_5)_2(dmso)_2]$ (1 g, 1.46 mmol), and the mixture was refluxed for 32 h. The resulting yellow-green solution was filtered through Celite and the filtrate was evaporated to a small volume (∼2 mL) and treated with *n*-hexane (10 mL) to give **2** as a dark yellow solid (0.85 g, 97%). Anal. Calcd for $C_{19}H_{14}F_5NOPtS$: C, 38.39; H, 2.37; N, 2.36; S, 5.39. Found: C, 38.72; H, 2.48; N, 2.34; S, 5.49%. MALDI-TOF (+): *m*/*z* (%) 516 $[Pt(C_6F_5)(ppy)]^+$ (19), 594 $[M]^+$ (100). IR (cm^{-1}): $\nu(C_6F_{5\ Xsens})$ 796 (m). ^1H NMR (δ, 400.17 MHz, CD_3COCD_3): 9.73 (d, J_{H-H} = 5.6, $^3J_{Pt-H}$ = 21.7, H^2_{ppy}), 8.14 (m, H^4_{ppy}, H^5_{ppy}), 7.76 (d, J_{H-H} = 7.8, H^6_{ppy}), 7.48 (t, J_{H-H} = 6.5, H^3_{ppy}), 7.10 (t, J_{H-H} = 7.5, H^7_{ppy}), 6.96 (t, J_{H-H} = 7.5, H^8_{ppy}), 6.41 (d, J_{H-H} = 7.5, $^3J_{Pt-H}$ = 62.4, H^9_{ppy}), 3.11 (s, $^3J_{Pt-H}$ = 14.9, 6H, $CH_{3\ dmso}$). ^{19}F NMR (δ, 376.5 MHz, CD_3COCD_3): −117.5 (d, $^3J_{Pt-F}$ = 494, 2 *o*-F), −163.1 (t, 1 *p*-F), −164.5 (m, 2 *m*-F). $^{13}C\{^1H\}$ NMR (δ, 100.6 MHz, CD_3COCD_3): 166.8 (s, $^1J_{Pt-C}$ = 81.7, C^{10}_{ppy}), 151.7 (s, C^2_{ppy}), 148.6 (dm, J_{C-F} = 231.2, C_{C6F5}), 147.8 (s, C^{12}_{ppy}), 146.6 (s, C^{11}_{ppy}), 141.0 (s, C^4_{ppy}), 136.8 (s, $^2J_{Pt-C}$ = 109.3, C^9_{ppy}), 130.6 (s, $^3J_{Pt-C}$ = 68.8, C^8_{ppy}), 126.2 (s, C^7_{ppy}), 124.7 (s, $^3J_{Pt-C}$ = 37.4, C^6_{ppy}), 124.1 (s, $^3J_{Pt-C}$ = 17.4, C^3_{ppy}), 120.3 (s, $^3J_{Pt-C}$ = 28.8, C^5_{ppy}), 45.32 (s, $^2J_{Pt-C}$ = 36.3, $CH_{3\ dmso}$).

Preparation of $[\{Pt(C_6F_5)(bzq)\}_2Pb(\mu\text{-}SpyCF_3\text{-}5)_2]$ (4). To a yellow suspension of $[Pb(SpyCF_3\text{-}5)_2]$, (0.070 g, 0.125 mmol) in CH_2Cl_2 (15 mL) was added 2 equiv of $[Pt(C_6F_5)(bzq)(OCMe_2)]$ (**1**; 0.150 g, 0.250 mmol). The resulting orange solution was stirred for 1 h and concentrated to a small volume (2 mL) to afford **4** as an orange solid (0.143 g, 70%). Anal. Calcd for $C_{50}H_{22}F_{16}N_4PbPt_2S_2$: C, 36.52; H, 1.35; N, 3.41; S, 3.90. Found: C, 36.41; H, 1.36; N, 3.17; S, 4.24%. MALDI-TOF (+): *m*/*z* (%) 718 $[Pt(C_6F_5)(bzq)(SpyCF_3)]^+$ (2), 925 $[Pt(C_6F_5)(bzq)Pb(SpyCF_3)]^+$ (100), 1465 $[\{Pt(C_6F_5)(bzq)\}_2Pb(SpyCF_3)]^+$ (3). IR (cm^{-1}): $\nu(C_6F_{5\ Xsens})$ 799 (s). ^1H NMR (δ, 400.17 MHz, CD_2Cl_2): 9.27 (s_{br}, H^2_{bzq}), 8.10 (d, J_{H-H} = 7.7, H^4_{bzq}), 7.75 (d, J_{H-H} = 8.7, $H^{5/6}_{bzq}$), 7.66 (d, J_{H-H} = 7.9, H^7_{bzq}), 7.43 (m, H^3_{bzq}, $H^{5/6}_{bzq}$, H^8_{bzq}, H^6_{SpyCF3}), 7.21 (d, J_{H-H} = 7.6, $H^{3/4}_{SpyCF3}$), 7.06 (d, J_{H-H} = 7.5, $H^{3/4}_{SpyCF3}$), 7.03 (d, J_{H-H} = 7.4, $^3J_{Pt-H}$ = 56.1, H^9_{bzq}). ^1H NMR (δ, 400.17 MHz, CD_3COCD_3): 9.25 (d, J_{H-H} = 4.8, $^3J_{Pt-H}$ = 26.5, H^2_{bzq}), 8.40 (d, J_{H-H} = 7.5, H^4_{bzq}), 7.85 (d, J_{H-H} = 8.7, $H^{5/6}_{bzq}$), 7.69 (d, J_{H-H} = 7.9, H^7_{bzq}), 7.60 (m, $H^{5/6}_{bzq}$, H^3_{bzq}), 7.57 (s, H^6_{SpyCF3}), 7.50 (d, J = 7.3, $H^{3/4}_{SpyCF3}$), 7.41 (t, J = 7.5, H^8_{bzq}), 7.21 (d, J = 7.3, $H^{3/4}_{SpyCF3}$), 7.03 (d, J_{H-H} = 6.9, $^3J_{Pt-H}$ = 57.5, H^9_{bzq}). ^{19}F NMR (δ, 376.5 MHz, 298 K, CD_2Cl_2): −63.1 (s, CF_3), −115.7 (br, 2 *o*-F), −124.8 (br, 2 *o*-F), −162.7 (t, 2 *p*-F), −164.0 (m_{br}, 4 *m*-F). ^{19}F NMR (δ, 376.5 MHz, 186 K, CD_2Cl_2): −62.8 (s, CF_3), −115.7 (d, $^3J_{Pt-F}$ = 384, 2 *o*-F), −124.6 (d, $^3J_{Pt-F}$ = 289, J_{Pb-F} = 1594, 2 *o*-F), −162.1 (t, 2 *p*-F), −162.8 (m, 2 *m*-F), −163.7 (m, 2 *m*-F). ^{19}F NMR (δ, 376.5 MHz, 298 K, CD_3COCD_3): −63.1 (s, CF_3), −118.5 (t, $^2J_{Pt-F}$ = 383, 4 *o*-F), −165.1 (t, 2 *p*-F), −165.8 (m, 4 *m*-F). The low solubility of this complex precludes its characterization by $^{13}C\{^1H\}$ NMR.

Preparation of $[\{Pt(C_6F_5)(ppy)\}_2Pb(\mu\text{-}Spy)_2]$ (5). To a suspension of $[Pb(Spy)_2]$ (0.072 g, 0.168 mmol) in CH_2Cl_2 (15 mL) was added 2 equiv of $[Pt(C_6F_5)(ppy)(dmso)]$ (**2**; 0.200 g, 0.336 mmol), and the initial yellow suspension was partially dissolved, giving rise to a red solution. The mixture was stirred for 1 h and filtered through Celite. The red solution was evaporated to a small volume (2 mL), and *n*-hexane was added (5 mL) to give an orange solid identified as **5** (0.176 g, 72%). Anal. Calcd for $C_{44}H_{24}F_{10}N_4PbPt_2S_2$: C, 36.19; H, 1.66; N, 3.84; S, 4.39. Found: C, 36.60; H, 1.97; N, 3.38; S, 4.21. MALDI-TOF (+): *m*/*z* (%) 626 $[Pt(C_6F_5)(ppy)(Spy)]^+$ (100), 833 $[Pt(C_6F_5)(ppy)Pb(Spy)]^+$ (39), 1350 $[\{Pt(C_6F_5)(bzq)\}_2Pb(Spy)]^+$ (41). IR (cm^{-1}): $\nu(C_6F_{5\ Xsens})$ 799 (vs). ^1H NMR (δ, 400.17 MHz, CD_2Cl_2): 8.72 (s_{br}, H^2_{ppy}), 7.78 (s, H^6_{Spy}), 7.63 (m, H^4_{ppy}, H^5_{ppy}), 7.58 (d, J_{H-H} = 7.6, H^6_{ppy}), 7.24 (s_{br}, H^4_{Spy}), 7.15 (t, J_{H-H} = 7.4, H^7_{ppy}), 7.03 (s_{br}, H^3_{Spy}), 7.01 (t, J_{H-H} = 7.2, H^3_{ppy}, H^8_{ppy}), 6.86 (s_{br}, H^5_{Spy}), 6.79 (d, J_{H-H} = 6.8, $^3J_{Pt-H}$ = 54.7, H^9_{ppy}). ^1H NMR (δ, 400.17 MHz, CD_3COCD_3): 8.73 (s_{br}, H^2_{ppy}), 7.94 (s_{br}, H^6_{Spy}), 7.91 (m, H^4_{ppy}, H^5_{ppy}), 7.73 (d, J_{H-H} = 7.5, H^6_{ppy}), 7.41 (t, J_{H-H} = 7.1, H^4_{Spy}), 7.13 (t, J_{H-H} = 7.3, H^7_{ppy}), 7.09 (s_{br}, H^3_{Spy}), 7.07 (m, H^3_{ppy}), 6.99 (t, J_{H-H} = 7.1, H^8_{ppy}), 6.94 (s_{br}, H^5_{Spy}), 6.80 (d, J_{H-H} = 7.2, $^3J_{Pt-H}$ = 59.4, H^9_{ppy}). ^{19}F NMR (δ, 376.5 MHz, 298 K, CD_2Cl_2): −120.0 (m_{br}, 4 *o*-F), −163.8 (t, 2 *p*-F), −164.5 (m, 4 *m*-F). ^{19}F NMR (δ, 376.5 MHz, 186 K, CD_2Cl_2): −116.1 (d, $^3J_{Pt-F}$ = 404, 2 *o*-F), −123.2 (d, $^3J_{Pt-F}$ = 317, J_{Pb-F} = 1557, 2 *o*-F), −163.1 (t, 2 *p*-F), −163.7 (m, 2 *m*-F), −164.1 (m, 2 *m*-F). ^{19}F NMR (δ, 282.4 MHz, 298 K, CD_3COCD_3): −117.9 (dm, $^3J_{Pt-F}$ = 408, 4 *o*-F), −164.9 (t, 2 *p*-F), −165.1 (m, 4 *m*-F). $^{13}C\{^1H\}$ NMR (δ, 100.6 MHz, CD_3COCD_3): 167.7 (s, C^{10}_{ppy}), 149.4 (s, C^2_{ppy}), 146.8 (s, C^6_{Spy}), 140.8 (s, C^5_{ppy}), 138.0 (s, C^4_{Spy}), 137.1 (s, C^9_{ppy}), 132.6 (s, C^3_{Spy}), 131.3 (s, C^8_{ppy}), 125.4 (s, $C^{6/7}_{ppy}$), 125.3 (s, $C^{6/7}_{ppy}$), 124.4 (s, C^3_{ppy}), 121.0 (s, C^5_{Spy}), 120.3 (s, C^4_{ppy}).

Preparation of $[\{Pt(C_6F_5)(ppy)\}_2Pb(\mu\text{-}SpyCF_3\text{-}5)_2]$ (6). This compound was obtained as a yellow solid (0.221 g, 82%) following a procedure similar to that described for **5**, using as starting precursors $[Pb(SpyCF_3\text{-}5)_2]$ (0.0948 g, 0.168 mmol) and $[Pt(C_6F_5)(ppy)(dmso)]$ (**2**; 0.200 g, 0.336 mmol). Anal. Calcd for $C_{46}H_{22}F_{16}N_4PbPt_2S_2$: C, 34.61; H, 1.39; N, 3.51; S, 4.02. Found: C, 34.59; H, 1.82; N, 3.93; S, 4.43%. MALDI-TOF (+): *m*/*z* (%) 695 $[Pt(C_6F_5)(ppy)(SpyCF_3)]^+$ (25), 901 $[Pt(C_6F_5)(ppy)Pb(SpyCF_3)]^+$ (100), 1418 $[\{Pt(C_6F_5)(bzq)\}_2Pb(SpyCF_3)]^+$ (10). IR (cm^{-1}): $\nu(C_6F_{5\ Xsens})$ 794 (vs). ^1H NMR (δ, 400.17 MHz, CD_2Cl_2): 8.93 (s_{br}, H^2_{ppy}), 7.86 (s_{br}, H^6_{SpyCF3}), 7.61 (s_{br}, H^4_{ppy}), 7.47 (s_{br}, H^5_{ppy}, H^6_{ppy}), 7.37 (d, J_{H-H} = 7.9, $H^{3/4}_{Spy}$), 7.15 (m, H^7_{ppy}, $H^{3/4}_{Spy}$), 7.04 (m, H^3_{ppy}, H^8_{ppy}), 6.83 (d, J_{H-H} = 6.7, $^3J_{Pt-H}$ = 60.9, H^9_{ppy}). ^1H NMR (δ, 400.17 MHz, CD_3COCD_3): 8.92 (d, J_{H-H} = 4.6, $^3J_{Pt-H}$ = 26.0, H^2_{ppy}), 8.20 (s_{br}, H^6_{SpyCF3}), 7.84 (d, J_{H-H} = 7.8, H^5_{ppy}), 7.81 (t, J_{H-H} = 7.7, H^4_{ppy}), 7.63 (t, J_{H-H} = 8.2, H^6_{ppy}, $H^{3/4}_{Spy}$), 7.30 (d, J_{H-H} = 5.4, $H^{3/4}_{Spy}$), 7.16 (t, J_{H-H} = 5.8, H^3_{ppy}), 7.10 (t, J_{H-H} = 7.2, H^7_{ppy}), 7.01 (t, J_{H-H} = 7.0, H^8_{ppy}), 6.84 (d, J_{H-H} = 7.3, $^3J_{Pt-H}$ = 57.5, H^9_{ppy}). ^{19}F NMR (δ, 376.5 MHz, 298 K, CD_2Cl_2): −62.8 (s, CF_3), −116.4 (br, 2 *o*-F), −123.7 (br, 2 *o*-F), −162.7 (t, 2 *p*-F), −163.9 (m, 4 *m*-F). ^{19}F NMR (δ, 376.5 MHz, 186 K, CD_2Cl_2): −62.1 (s, CF_3), −115.9 (d, $^3J_{Pt-F}$ = 387, 2 *o*-F), −123.1 (br, 2 *o*-F), −162.5 (t, 2 *p*-F), −163.0 (m, 2 *m*-F), −164.0 (m, 2 *m*-F). ^{19}F NMR (δ, 376.5 MHz, CD_3COCD_3): −64.6 (s, CF_3), −117.5 (m, $^3J_{Pt-F}$ = 382, 4 *o*-F), −164.4 (t, 2 *p*-F), −165.0 (m, 4 *m*-F). $^{13}C\{^1H\}$ NMR (δ, 100.6 MHz, CD_3COCD_3): 171.3 (s_{br}, C^2_{SpyCF3}), 167.4 (s, $^1J_{Pt-C}$ = 76.8, C^{10}_{ppy}), 150.8 (dm, $^1J_{C-F}$ = 235.2, C_{C6F5}), 149.9 (s, C^2_{ppy}), 148.3 (dm, $^1J_{C-F}$ = 232.1, C_{C6F5}), 147.3 (s, $C^{11/12}_{ppy}$), 146.6 (s, $C^{11/12}_{ppy}$) 143.9 (s, C^6_{SpyCF3}), 141.1 (s, C^5_{ppy}), 137.4 (dm, $^1J_{C-F}$ = 247.8, C_{C6F5}), 137.3 (s, $^2J_{Pt-C}$ = 96.6, C^9_{ppy}), 133.7 (s, C^3_{SpyCF3}), 132.4 (s, C^4_{SpyCF3}), 131.4 (s, $^3J_{Pt-C}$ = 66.8, C^8_{ppy}), 125.7 (s, C^7_{ppy}), 125.3 (s, $^3J_{Pt-C}$ = 37.2, C^6_{ppy}), 124.7 (q, J_{C-F} = 271, C_{CF3}), 124.5 (s, $^3J_{Pt-C}$ = 18.4, C^3_{ppy}), 122.6 (q, $^2J_{C-F}$ = 32.4, C^5_{Spy}), 120.1 (s, $^3J_{Pt-C}$ = 26.7, C^4_{ppy}).

X-ray Crystallography. Details of the X-ray analyses are summarized in Tables S10 and S11 (Supporting Information). Suitable monocrystals for X-ray diffraction were obtained as follows: greenish yellow (**2**) and orange (**4**·0.9CH_2Cl_2, **6**·**acetone**) crystals

dx.doi.org/10.1021/ic501458q | *Inorg. Chem.* 2014, 53, 8770−8785

were obtained by slow diffusion at −30 °C of *n*-hexane into solutions of the complexes in CH_2Cl_2 (**2**, **4**) or acetone (**6**), respectively. Yellow (**4**·(**acetone**)$_{1.5}$, **6**·4C_6H_6, **6**·4$CHCl_3$) or orange (**5**·2$CHCl_3$, **6**·2CH_2Cl_2) crystals were obtained by slow evaporation at 4 °C of the corresponding saturated solutions of the complexes in acetone (**4**), chloroform (**5**), benzene (**6**), or dichloromethane (**6**) or by cooling to −30 °C a saturated solution of complex **6** in chloroform (**6**·4$CHCl_3$). In all cases, graphite-monochromated Mo Kα radiation was used. For **2** and **6**·**acetone**, the data were acquired with an Oxford Diffraction Xcalibur CCD diffractometer, and the diffraction frames were integrated and corrected for absorption using the Crysalis RED package.[24] For the rest of the structures, X-ray intensity data were collected with a NONIUS-κCCD area-detector diffractometer and images processed using the DENZO and SCALEPACK suite of programs,[25] carrying out the absorption correction at this point for complexes **4**·0.9CH_2Cl_2, **5**·2$CHCl_3$, **6**·4C_6H_6, **6**·2CH_2Cl_2, and **6**·4$CHCl_3$. For **4**·(**acetone**)$_{1.5}$, the absorption correction was performed using SORTAV.[26] The structures were solved by direct methods or Patterson methods using SHELXS-97[27] (**2**, **4**·(**acetone**)$_{1.5}$, **5**·2$CHCl_3$, and **6**·**acetone**) or SIR-2004[28] (**4**·0.9CH_2Cl_2, **6**·4$CHCl_3$, **6**·4C_6H_6, and **6**·2CH_2Cl_2) and refined by full-matrix least-squares on F^2 with SHELXL-97.[27] All non-hydrogen atoms were assigned anisotropic displacement parameters. All hydrogen atoms were constrained to idealized geometries, fixing isotropic displacement parameters at 1.2 times the U_{iso} value of their attached carbon for the aromatic and methylene carbons and 1.5 times the U_{iso} value for the methyl groups. For the complex **4**·(**acetone**)$_{1.5}$, which crystallizes in the non-centrosymmetric space group $P2_1$, the crystal chosen for this structural analysis was found to be a merohedric twin, as confirmed by the absolute structure parameter (0.456(6)). Inspection of the symmetry (using Platon[29]) did not suggest any obvious space group change. For **4**·0.9CH_2Cl_2 and **6**·2CH_2Cl_2, disordered crystallization molecules of CH_2Cl_2 were observed but could not be properly modeled. Both structures were examined with PLATON[29,30] and SQUEEZE.[29,31] In the case of **4**·0.9CH_2Cl_2, the presence of two voids of 835 Å^3 in the unit cell was revealed, each of them containing 135e, which fits well with the presence of 7 molecules of CH_2Cl_2 in the unit cell. Therefore, we have included them in the empirical formula as crystallization solvent (**4**·0.9CH_2Cl_2). In the case of **6**·2CH_2Cl_2, it the presence of six voids in the unit cell was revealed, containing a total of 490e, which fits well with the presence of 12 molecules of CH_2Cl_2 in the unit cell. Therefore, we have also included them in the empirical formula as crystallization solvent (**6**·2CH_2Cl_2). Several restraints have been used in order to model positional disorders in crystallization solvents (**5**·2$CHCl_3$, 0.70/0.30, 0.60/0.40; **6**·4$CHCl_3$, 0.60/0.40) or in one CF_3 group (**4**·0.9CH_2Cl_2, 0.70/0.30; **4**·(**acetone**)$_{1.5}$, 0.55/0.45; **6**·4C_6H_6, 0.70/0.30; **6**·2CH_2Cl_2, 0.50/0.50). Finally, the structures of **2**, **4**·(**acetone**)$_{1.5}$, **5**·2$CHCl_3$, **6**·2CH_2Cl_2, and **6**·4$CHCl_3$ show some residual peaks greater than 1 e Å^{-3} in the vicinity of the platinum atoms or the crystallization solvent, but with no chemical meaning.

Computational Details for DFT Calculations. DFT and TD-DFT calculations were performed on the solvated and unsolvated complexes **4** and **6** using Gaussian 09 (revision B.01).[32] Geometries in the S^0 ground state were optimized using the B3LYP method and in the T^1 excited state using the unrestricted U-B3LYP Becke three-parameter functional combined with the Lee−Yang−Parr correlation functional.[33] The geometries obtained in the crystal structures (**4**·(0.9CH_2Cl_2), **4**·(**acetone**)$_{1.5}$ molecule **B**, **6**·4$CHCl_3$, and **6**·(**acetone**)) were used as starting points in the ground-state optimizations. The basis set used for the platinum and lead centers was the LanL2DZ effective core potential and 6-31G(d,p) for the ligand atoms.[34]

■ ASSOCIATED CONTENT

Supporting Information

Tables, figures, and CIF and xyz files giving crystallographic, photophysical, and theoretical data for all compounds prepared in this paper. This material is available free of charge via the Internet at http://pubs.acs.org.

■ AUTHOR INFORMATION

Corresponding Authors

*E.L.: e-mail, elena.lalinde@unirioja.es; tel, (+34)941-299643, (+34)941-299645.

*M.T.M.: e-mail, teresa.moreno@unirioja.es.

Present Address

[‖]Department of Chemistry, Institute for Advanced Studies in Basic Sciences (IASBS), Zanjan 45137-66731, Iran.

Notes

The authors declare no competing financial interest.

■ ACKNOWLEDGMENTS

This work was supported by the Spanish MICINN (CTQ2008-06669-C02-01,02/BQU and a grant for S.R.). The authors thank the CESGA for computer support.

■ REFERENCES

(1) (a) Braunstein, P.; Oro, L. A.; Raithby, P. R. *Metal Clusters in Chemistry*; Wiley-VCH: New York, 1999. (b) Berry, J. F. In *Metal-Metal Bonding*; Parkin, G., Mingos, D. M. P., Eds.; Springer-Verlag: Berlín, 2010; Structure and Bonding Vol. *136*. (c) Balch, A. L. In *Metal-Metal Bonds and Clusters in Chemistry*; Fackler, J. P. J., Ed.; Plenum: New York, 1990.

(2) (a) Chen, Z. N.; Zhao, N.; Fan, Y.; Ni, J. *Coord. Chem. Rev.* **2009**, *253*, 1. (b) Díez, Á.; Lalinde, E.; Moreno, M. T. *Coord. Chem. Rev.* **2011**, *255*, 2426. (c) Puntoriero, F. *Photochemistry* **2011**, *39*, 65. (d) Yam, V. W.-W.; Lo, K. K. W.; Wong, K. M.-C. *J. Organomet. Chem.* **1999**, *578*, 3.

(3) (a) Schmidbaur, H.; Schier, A. *Chem. Soc. Rev.* **2012**, *41*, 370. (b) Sculfort, S.; Braunstein, P. *Chem. Soc. Rev.* **2011**, *40*, 2741. (c) Schmidbaur, H.; Schier, A. *Chem. Soc. Rev.* **2008**, *37*, 1931. (d) Katz, M. J.; Sakai, K.; Leznoff, D. B. *Chem. Soc. Rev.* **2008**, *37*, 1884. (e) Mak, T. C. W.; Zhao, X.-L.; Wang, Q.-M.; Guo, G.-C. *Coord. Chem. Rev.* **2007**, *251*, 2311. (f) Murahashi, T.; Kurosawa, H. *Coord. Chem. Rev.* **2002**, *231*, 207. (g) Kajitani, Y.; Tsuge, K.; Sasaki, Y.; Kato, M. *Chem. Eur. J.* **2012**, *18*, 11196. (h) Anderson, B. M.; Hurst, S. K. *Eur. J. Inorg. Chem.* **2009**, *21*, 3041. (i) Doerrer, L. H. *Dalton Trans.* **2010**, *39*, 3543. (j) Bauer, J.; Braunschweig, H.; Dewhurst, R. D. *Chem. Rev.* **2012**, *112*, 4329.

(4) (a) Mayoral-Muñoz, M. J.; Fernández, G. *Chem. Sci.* **2012**, *3*, 1395. (b) Tanaka, Y.; Wong, K. M.-C.; Yam, V. W.-W. *Chem. Sci.* **2012**, *3*, 1185. (c) Leung, S. Y.-L.; Tam, A. Y.-Y.; Tao, C.-H.; Chow, H. S.; Yam, V. W.-W. *J. Am. Chem. Soc.* **2012**, *134*, 1047. (d) Wong, K. M.-C.; Yam, V. W.-W. *Acc. Chem. Res.* **2011**, *44*, 424.

(5) (a) Che, C.-M.; Lai, S.-W. Luminescence and Photophysics of Gold Complexes. In *Gold Chemistry*; Mohr, F., Ed.; Wiley-VCH: Weinheim, Germany, 2009. (b) López-de-Luzuriaga, J. M. Luminescence of Supramolecular Gold-Containing Materials. In *Modern Supramolecular Gold Chemistry: Gold-Metal Interactions and Applications*; Laguna, A., Ed.; Wiley-VCH: Weinheim, Germany, 2008. (c) He, X.; Yam, V. W. W. *Coord. Chem. Rev.* **2011**, *255*, 211. (d) Zhang, X.; Li, B.; Chen, Z. H.; Chen, Z. N. *J. Mater. Chem.* **2012**, *22*, 11427. (e) Yam, V. W.-W.; Wong, K. M.-C. *Chem. Commun.* **2011**, *47*, 11579. (f) Lima, J. C.; Rodriguez, L. *Chem. Soc. Rev.* **2011**, *40*, 5442. (g) Yam, V. W.-W.; Cheng, E. C.-C. *Chem. Soc. Rev.* **2008**, *37*, 1806. (h) Tiekink, E. R. T.; Kang, J.-G. *Coord. Chem. Rev.* **2009**, *253*, 1627. (i) Wong, K. M.-C.; Yam, V. W.-W. *Coord. Chem. Rev.* **2007**, *251*, 2477. (j) Kato, M. *Bull. Chem. Soc. Jpn.* **2007**, *80*, 287. (k) Berenguer, J. R.; Lalinde, E.; Moreno, M. T. *Coord. Chem. Rev.* **2010**, *254*, 832. (l) Fernández, E. J.; Laguna, A.; López-de-Luzuriaga, J. M. *Dalton Trans.* **2007**, 1969. (m) Fernández, E. J.; Laguna, A.; López-de-Luzuriaga, J. M. *Coord. Chem. Rev.* **2005**, *249*, 1423. (n) Wong, K. M.-C.; Hui, C.-K.; Yu, K.-L.; Yam, V. W.-W. *Coord. Chem. Rev.* **2002**, *229*, 123. (o) Yam, V. W.-W. *J. Organomet. Chem.* **2004**, *689*, 1393. (p) Chen, Z.-N.; Fan, Y.; Ni, J. *Dalton Trans.* **2008**, 573.

(6) Chen, Z.-N.; Zhao, N.; Fan, Y.; Ni, J. *Coord. Chem. Rev.* **2009**, *253*, 1.
(7) (a) Zhao, Q.; Li, F.; Huang, C. *Chem. Soc. Rev.* **2010**, *39*, 3007. (b) Wenger, O. S. *Chem. Rev.* **2013**, *113*, 3686. (c) Shan, G.-G.; Li, H.-B.; Cao, H.-T.; Zhu, D.-X.; Li, P.; Su, Z.-M.; Liao, Y. *Chem. Commun.* **2012**, *48*, 2000. (d) Lefebvre, J.; Korcok, J. L.; Katz, M. J.; Leznoff, D. B. *Sensors* **2012**, *12*, 3669.
(8) (a) Balch, A. L. *Angew. Chem., Int. Ed.* **2009**, *48*, 2641. (b) Zhang, X.; Chi, Z.; Zhang, Y.; Liu, S.; Xu, J. *J. Mater. Chem. C* **2013**, *1*, 3376. (c) Ni, J.; Zhang, X.; Wu, Y.-H.; Zhang, L.-Y.; Chen, Z.-N. *Chem. Eur. J.* **2011**, *17*, 1171. (d) Lasanta, T.; Olmos, M. E.; Laguna, A.; López-de-Luzuriaga, J. M.; Naumov, P. *J. Am. Chem. Soc.* **2011**, *133*, 16358. (e) Osawa, M.; Kawata, I.; Igawa, S.; Hoshino, M.; Fukunaga, T.; Hashizume, D. *Chem. Eur. J.* **2010**, *16*, 12114.
(9) (a) Rachford, A. A.; Castellano, F. N. *Inorg. Chem.* **2009**, *48*, 10865. (b) Forniés, J.; Fuertes, S.; Martín, A.; Sicilia, V.; Gil, B.; Lalinde, E. *Dalton Trans.* **2009**, 2224. (c) Falvello, L. R.; Forniés, J.; Garde, R.; García, A.; Lalinde, E.; Moreno, M. T.; Steiner, A.; Tomás, M.; Usón, I. *Inorg. Chem.* **2006**, *45*, 2543. (d) Omary, M. A.; Mohamed, A. A.; Rawashdeh-Omary, M. A.; Fackler, J. P., Jr. *Coord. Chem. Rev.* **2005**, *249*, 1372.
(10) (a) Lefebvre, J.; Batchelor, R. J.; Leznoff, D. B. *J. Am. Chem. Soc.* **2004**, *126*, 16117. (b) Strasser, C. E.; Catalano, V. J. *J. Am. Chem. Soc.* **2010**, *132*, 10009. (c) Laguna, A.; Lasanta, T.; López-de-Luzuriaga, J. M.; Monge, M.; Naumov, P.; Olmos, M. E. *J. Am. Chem. Soc.* **2010**, *132*, 456. (d) Fernández, E. J.; López-de-Luzuriaga, J. M.; Monge, M.; Olmos, M. E.; Puelles, R. C.; Laguna, A.; Mohamed, A. A.; Fackler, J. P., Jr. *Inorg. Chem.* **2008**, *47*, 8069.
(11) Maliarik, M.; Nagle, J. K.; Ilyukhin, A.; Murashova, E.; Mink, J.; Skripkin, M.; Glaser, J.; Kovacs, M.; Horváth, A. *Inorg. Chem.* **2007**, *46*, 4642.
(12) (a) Jamali, S.; Ashtiani, M. M.; Jamshidi, Z.; Lalinde, E.; Moreno, M. T.; Samouei, H.; Escudero-Adán, E.; Benet-Bucholz, J. *Inorg. Chem.* **2013**, *52*, 10729. (b) Catalano, V. J.; Bennett, B. L.; Yson, R. L.; Noll, B. C. *J. Am. Chem. Soc.* **2000**, *122*, 10056. (c) Catalano, V. J.; Bennett, B. L.; Muratidis, S.; Noll, B. C. *J. Am. Chem. Soc.* **2001**, *123*, 173. (d) Catalano, V. J.; Malwitz, M. A. *J. Am. Chem. Soc.* **2004**, *126*, 6560. (e) Ara, I.; Berenguer, J. R.; Forniés, J.; Gómez, J.; Lalinde, E.; Martín, A.; Merino, R. *Inorg. Chem.* **1997**, *36*, 6461. (f) Berenguer, J. R.; Forniés, J.; Gómez, J.; Lalinde, E.; Moreno, M. T. *Organometallics* **2001**, *20*, 4847. (g) Charmant, J. P. H.; Forniés, J.; Gómez, J.; Lalinde, E.; Merino, R. I.; Moreno, M. T.; Orpen, A. G. *Organometallics* **2003**, *22*, 652. (h) Berenguer, J. R.; Forniés, J.; Gil, B.; Lalinde, E. *Chem. Eur. J.* **2006**, *12*, 785. (i) Díez, Á.; Fernández, J.; Lalinde, E.; Moreno, M. T.; Sánchez, S. *Inorg. Chem.* **2010**, *49*, 11606. (j) Díez, A.; Forniés, J.; Gómez, J.; Lalinde, E.; Martín, A.; Moreno, M. T.; Sánchez, S. *Dalton Trans.* **2007**, 3653. (k) Forniés, J.; García, A.; Lalinde, E.; Moreno, M. T. *Inorg. Chem.* **2008**, *47*, 3651. (l) Belío, Ú.; Fuertes, S.; Martín, A. *Inorg. Chem.* **2013**, *52*, 5627. (m) Usón, R.; Forniés, J.; Tomás, M.; Garde, R.; Merino, R. I. *Inorg. Chem.* **1997**, *36*, 1383. (n) Wu, G.; Wang, D. *J. Cluster Sci.* **2007**, *18*, 406. (o) Nagle, J. K.; Balch, A. L.; Olmstead, M. M. *J. Am. Chem. Soc.* **1988**, *110*, 319. (p) Stork, J. R.; Olmstead, M. M.; Balch, A. L. *J. Am. Chem. Soc.* **2005**, *127*, 6512. (q) Stork, J. R.; Olmstead, M. M.; Fettinger, J. C.; Balch, A. L. *Inorg. Chem.* **2006**, *45*, 849. (r) Balch, A. L.; Rowley, S. P. *J. Am. Chem. Soc.* **1990**, *112*, 6139. (s) Renn, O.; Lippert, B.; Mutikainen, I. *Inorg. Chim. Acta* **1993**, *208*, 219. (t) Oberbeckmann-Winter, N.; Braunstein, P.; Welter, R. *Organometallics* **2004**, *23*, 6311. (u) Song, H. B.; Zhang, Z. Z.; Hui, H.; Che, C. M.; Mak, T. C. W. *Inorg. Chem.* **2002**, *41*, 3146. (v) Quadrelli, E. A.; Davies, J. E.; Johnson, B. F. G.; Feeder, N. *Chem. Commun.* **2000**, 1031. (w) Chen, W.; Liu, F.; Xu, D. X.; Matsumoto, K.; Kishi, S.; Kato, M. *Inorg. Chem.* **2006**, *45*, 5552.
(13) (a) Catalano, V. J.; Bennett, B. L.; Kar, H. M.; Noll, B. C. *J. Am. Chem. Soc.* **1999**, *121*, 10235. (b) Fernández, E. J.; Laguna, A.; Lasanta, T.; López-de-Luzuriaga, J. M.; Montiel, M.; Olmos, M. E. *Organometallics* **2008**, *27*, 2971. (c) Fernández, E. J.; López-de-Luzuriaga, J. M.; Olmos, M. E.; Pérez, J.; Laguna, A.; Lagunas, M. C. *Inorg. Chem.* **2005**, *44*, 6012. (d) Fernández, E. J.; Laguna, A.; López-de-Luzuriaga, J. M.; Monge, M.; Montiel, M.; Olmos, M. E. *Inorg. Chem.* **2007**, *46*, 2935. (e) Fernéndez, E. J.; Garau, A.; Laguna, A.; Lasanta, T.; Lippolis, V.; López-de-Luzuriaga, J. M.; Montiel, M.; Olmos, M. E. *Organometallics* **2010**, *29*, 2951. (f) Fernández, E. J.; Laguna, A.; López-de-Luzuriaga, J. M.; Montiel, M.; Olmos, M. E.; Pérez, J. *Organometallics* **2005**, *24*, 1631.
(14) (a) Balch, A. L.; Fung, E. Y.; Nagle, J. K.; Olmstead, M. M.; Rowley, S. P. *Inorg. Chem.* **1993**, *32*, 3295. (b) Usón, R.; Forniés, J.; Falvello, L. R.; Usón, M. A.; Usón, I. *Inorg. Chem.* **1992**, *31*, 3697. (c) Albano, V. G.; Castellari, C.; Monari, M.; De Felice, V.; Ferrara, M. L.; Ruffo, F. *Organometallics* **1995**, *14*, 4213. (d) Ara, I.; Falvello, L. R.; Forniés, J.; Gómez-Cordón, J.; Lalinde, E.; Merino, R. I.; Usón, I. *J. Organomet. Chem.* **2002**, *663*, 284. (e) Casas, J. M.; Forniés, J.; Martín, A.; Orera, V. M.; Orpen, A. G.; Rueda, A. *Inorg. Chem.* **1995**, *34*, 6514. (f) Catalano, V. J.; Bennett, B. L.; Noll, B. C. *Chem. Commun.* **2000**, 1413. (g) Heitmann, D.; Pape, T.; Hepp, A.; Mück-Lichtenfeld; Grimme, S.; Ekkehardt-Hahn, F. *J. Am. Chem. Soc.* **2011**, *133*, 11118. (h) Braunschweig, H.; Damme, A.; Dewhurst, R. D.; Hupp, F.; Jiménez-Halla, J. O. C.; Radacki, K. *Chem. Commun.* **2012**, *48*, 10410.
(15) (a) Shimoni-Liuny, L.; Glusker, J. P.; Bock, C. W. *Inorg. Chem.* **1998**, *37*, 1853. (b) Davidovich, R. L.; Stavila, V.; Marinin, D. V.; Voit, E. I.; Whitmire, K. H. *Coord. Chem. Rev.* **2009**, *253*, 1316. (c) Davidovich, R. L.; Stavila, V.; Whitmire, K. H. *Coord. Chem. Rev.* **2010**, *254*, 2193. (d) Gourlaouen, C.; Gérard, H.; Piquemal, J.-P.; Parisel, O. *Chem. Eur. J.* **2008**, *14*, 2730. (e) Greer, B. J.; Michaelis, V. K.; Katz, M. J.; Leznoff, D. B.; Schreckenbach, G.; Kroeker, S. *Chem. Eur. J.* **2011**, *17*, 3609.
(16) Berenguer, J. R.; Díez, A.; Fernández, J.; Forniés, J.; García, A.; Gil, B.; Lalinde, E.; Moreno, M. T. *Inorg. Chem.* **2008**, *47*, 7703.
(17) Berenguer, J. R.; Fernández, J.; Gil, B.; Lalinde, E.; Sánchez, S. *Chem. Eur. J.* **2014**, *20*, 2574.
(18) Berenguer, J. R.; Lalinde, E.; Martin, A.; Moreno, M. T.; Ruiz, S.; Sánchez, S.; Shahsavari, H. R. *Chem. Commun.* **2013**, *49*, 5067.
(19) (a) Berenguer, J. R.; Lalinde, E.; Moreno, M. T.; Sánchez, S.; Torroba, J. *Inorg. Chem.* **2012**, *51*, 11665. (b) Martín, A.; Belío, Ú.; Fuertes, S.; Sicilia, V. *Eur. J. Inorg. Chem.* **2013**, *2013*, 2231. (c) Sasaki, I.; Bijani, C.; Ladeira, S.; Bourdon, V.; Faller, P.; Hureau, C. *Dalton Trans.* **2012**, *41*, 6404. (d) Owen, J. S.; Labinger, J. A.; Bercaw, J. E. *J. Am. Chem. Soc.* **2004**, *126*, 8247. (e) Newman, C. P.; Casey-Green, K.; Clarkson, G. J.; Cave, G. W. V.; Errington, W.; Rourke, J. P. *Dalton Trans.* **2007**, 3170. (f) Ghavale, N.; Wadawale, A.; Dey, S.; Jain, V. K. *J. Organomet. Chem.* **2010**, *695*, 1237. (g) Yagyu, T.; Ohashi, J.-i.; Maeda, M. *Organometallics* **2007**, *26*, 2383. (h) Rao, Y.-L.; Wang, S. *Inorg. Chem.* **2009**, *48*, 7698.
(20) Sousa-Pedrares, A.; Casanova, M. I.; García-Vázquez, J. A.; Durán, M. L.; Romero, J.; Sousa, A.; Silver, J.; Titler, P. J. *Eur. J. Inorg. Chem.* **2003**, 678.
(21) (a) Rekken, B. D.; Brown, T. M.; Olmstead, M. M.; Fettinger, J. C.; Power, P. P. *Inorg. Chem.* **2013**, *52*, 3054. (b) Rossini, A. J.; Macgregor, A. W.; Smith, A. S.; Schatte, G.; Schurko, R. W.; Briand, G. G. *Dalton Trans.* **2013**, *42*, 9533.
(22) We note that in this work we accept 3.20 Å as the upper limit of the Pb−F distance. At values above this we consider the Pb−F distances negligible. The limit is below the van der Waals limit (Pb^{II}···F 3.46 Å), but it is longer than the sum of the covalent radius of Pb (1.46 Å) and van der Waals radius of F (1.47 Å) (2.93 Å) and of course longer than the primary coordination sphere of the Pb^{II} atom, which can be considered as the sum of ionic radii of Pb^{II} (CN 6, 1.19 Å and F^- 1.285 Å (2.475 Å)).
(23) Makal, A.; Benedict, J.; Trzop, E.; Sokolow, J.; Fournier, B.; Chen, Y.; Kalinowski, J. A.; Graber, T.; Henning, R.; Coppens, P. *J. Phys. Chem. A* **2012**, *116*, 3359.
(24) *CrysAlisRED: A Program for Xcalibur CCD System X-Ray Diffraction Data Reduction*; Oxford Diffraction, Oxford, U.K., 2005.
(25) Otwinowski, Z.; Minor, W. In *Methods in Enzymology*; Carter, C. V., Jr., Sweet, R. M., Eds.; Academic Press: New York, 1997; Vol. *276A*, p 307.
(26) Blessing, R. H. *Acta Crystallogr., Sect. A* **1995**, *A51*, 33.
(27) Sheldrick, G. M. *SHELX-97, a program for the refinement of crystal structures*; University of Göttingen, Göttingen, Germany, 1997.

(28) Burla, M. C.; Caliandro, R.; Camalli, M.; Carrozzini, B.; Cascarano, G. L.; De Caro, L.; Giacovazzo, C.; Polidori, G.; Spagna, R. *J. Appl. Crystallogr.* **2005**, *38*, 381.
(29) Spek, A. L. *Acta Crystallogr., Sect. A* **1990**, *A46*, c34.
(30) Spek, A. L. PLATON, A Multipurpose Crystallographic Tool; Utrecht University, Utrecht, The Netherlands, 1998.
(31) Spek, A. L. *SQUEEZE, incorporated into PLATON: A Multipurpose Crystallographic Tool*; University of Utrecht, Utrecht, The Netherlands, 2005.
(32) Frisch, M. J.; et al. *Gaussian 03, Revision E.01*: Gaussian, Inc., Wallingford, CT, 2004 (see the Supporting Information for the complete citation).
(33) (a) Becke, A. D. *Phys. Rev. A* **1988**, *38*, 3098. (b) Becke, A. D. *J. Chem. Phys.* **1993**, *98*, 5648. (c) Lee, C.; Yang, W.; Parr, R. G. *Phys. Rev.* **1988**, *B37*, 785.
(34) Wadt, W. R.; Hay, P. J. *J. Chem. Phys.* **1985**, *82*, 284.